NASA Technical Memorandum 4752

Biomechanically Induced and Controller Coupled Oscillations Experienced on the F-16XL Aircraft During Rolling Maneuvers

John W. Smith and Terry Montgomery
Dryden Flight Research Center
Edwards, California

National Aeronautics and
Space Administration
Office of Management
Scientific and Technical
Information Program
1996

ABSTRACT

During rapid rolling maneuvers, the F-16 XL aircraft exhibits a 2.5 Hz lightly damped roll oscillation, perceived and described as "roll ratcheting." This phenomenon is common with fly-by-wire control systems, particularly when primary control is derived through a pedestal-mounted sidearm controller. Analytical studies have been conducted to model the nature of the integrated control characteristics. The analytical results complement the flight observations. A three-degree-of-freedom linearized set of aerodynamic matrices was assembled to simulate the aircraft plant. The lateral–directional control system was modeled as a linear system. A combination of two second-order transfer functions was derived to couple the lateral acceleration feedthrough effect of the operator's arm and controller to the roll stick force input. From the combined systems, open-loop frequency responses and a time history were derived, describing and predicting an analogous in-flight situation. This report describes the primary control, aircraft angular rate, and position time responses of the F-16 XL-2 aircraft during subsonic and high-dynamic-pressure rolling maneuvers. The analytical description of the pilot's arm and controller can be applied to other aircraft or simulations to assess roll ratcheting susceptibility.

INTRODUCTION

During rolling maneuvers and tracking tasks, many modern fighter aircraft tend to experience roll instabilities or damped oscillations. These oscillations are noticeable at initiation and recovery following large primary roll control commands. Large roll rate commands require high gradient gains and high roll acceleration to achieve and to recover from the roll in a desired manner. The periodic motions that often follow are sustained by the pilot/vehicle coupled interactions. Pilots and investigators generally refer to these interactions as either pilot-induced oscillations (PIOs) or "roll ratcheting." The brief discussion that follows attempts to distinguish between the two.

Usually, PIOs predominate during tracking tasks or following large, rapid control inputs. For example, during a tracking task, the pilot is actively minimizing the error or command signal. If the product of the pilot's gain and the system gain increases sufficiently, then the pilot/vehicle closed-loop system tends toward neutral stability. Neutral stability PIOs most often develop at a crossover frequency within the range of 0.5 to 1.0 Hz.

Roll ratcheting predominates during roll recovery and is generally associated with or caused by an interaction of the dynamic characteristics of the neuromuscular limb system, the aircraft, and the mechanical controller. The biomechanical nature of the phenomenon is similar to a "bobweight" in its feedthrough effect and produces oscillations within a frequency range of 2 to 3 Hz. The magnitude and damping are governed by the arm weight, the controller weight, the wrist interface, and the control system gain (primarily the commanded roll gradient gain).

During the F-16 XL-2 functional test flight phase, a minimal number of rapid rolling maneuvers and recovery tests were conducted. At the end of the final functional test flight, the copilot, maneuvering and maintaining control from the aft seat, initiated and completed three rapid 360° rolling maneuvers at Mach 0.9 and an altitude of 11,600 ft. During the roll recovery portion, as the copilot attempted to capture a desired roll angle, the aircraft exhibited a considerable amount of lightly damped roll oscillations. These oscillations continued through more than 10 cycles at a frequency of 2.5 Hz. Particularly important, the roll controller force transducer (measured at the controller) recorded the same characteristic oscillations as other aircraft control and response parameters. Based on the flight experience and confirmed feedthrough effects existing at the controller, the observed phenomenon was believed to offer a good example of roll ratcheting for analysis and reporting.

Similar phenomena were encountered during other flight test programs.[1–5] The Air Force conducted F-16 XL rolling maneuver evaluations. At Mach 0.9 at an altitude of 5200 ft, their pilots experienced roll ratcheting. Tracking studies using a variable-stability aircraft showed that roll ratcheting tendencies increase as augmented roll damping is increased and that pilot rating increases correspondingly.[4, 5] Using simulation and analytical studies where tracking tasks were generated by comparing position or target feedbacks to a forcing function, the problem has been defined and investigated extensively.[6–10]

In addition to presenting the actual flight data, this report also analyzes the biomechanical nature of the "bobweight" feedthrough effect and associated phenomenon. Linear models of the aircraft dynamics, control system, and the arm, wrist, and controller were combined to model the phenomenon.

A mathematical model and description for the pilot's arm and controller were developed. Extensive use was made of existing data to define the wrist and arm

dynamic characteristics.[10] These characteristics include wrist damping, spring constants, pilot's arm equivalent weight, frequency, and damping. Previous tests had been conducted with the pilot partially restrained on a vibrating platform while performing single-axis tracking tasks.[10] Various controllers were firmly mounted to the vibrating platform. From these tests, the biodynamic constants and coefficients for the arm and wrist interface compliance were determined. The combination of limb dynamics, controller dynamics, and their equivalent weight effects are referred to as the manipulation dynamics. The mathematical description of the manipulation dynamics was concatenated with and integrated into the aircraft aerodynamics and augmentation systems.

A linear mathematical model for the integrated aircraft aerodynamics and augmentation systems was derived. The aircraft derivatives used to define the plant were available from previously reported flight results.[3,11–14] Wind-tunnel data for individually measured control derivatives were also available.[14] The complete set of dimensional derivatives, as defined in appendixes A and B, was assembled as matrices in a state-space format. Using a FORTRAN control program,[15] open-loop frequency responses and a typical time history were calculated.

This report describes the F-16 XL-2 roll ratcheting in-flight experience. Mathematical and theoretical analyses are presented to describe and predict the characteristics of the roll ratcheting phenomenon caused by a "bobweight" feedthrough effect. The flight test results and analytical predictions reported here were conducted at the NASA Dryden Flight Research Center, Edwards, California.

VEHICLE DESCRIPTION

The following sections provide a general description of the basic F-16 XL aircraft and aircraft control systems. Instrumentation and recording systems used to obtain the flight data were developed by NASA Dryden.

Aircraft

Two F-16 XL aircraft were designed and built by General Dynamics (Fort Worth, Texas) for a U.S. Air Force contract. The aircraft were initially considered prototypes, emphasizing the multirole fighter capability. At the start of the flight test phase, these aircraft were formally referred to as demonstrators. Both aircraft are modifications of the F-16 A/B aircraft. The forward and midfuselage have been extended by 56 in. The design planform incorporated a cranked arrow wing. The number 2 aircraft, of concern in this report, is a two-seat fighter using an F-110 GE-129 engine (General Electric, Lynn, Massachusetts) at the time of flight 12. Figure 1 shows the relative size and location

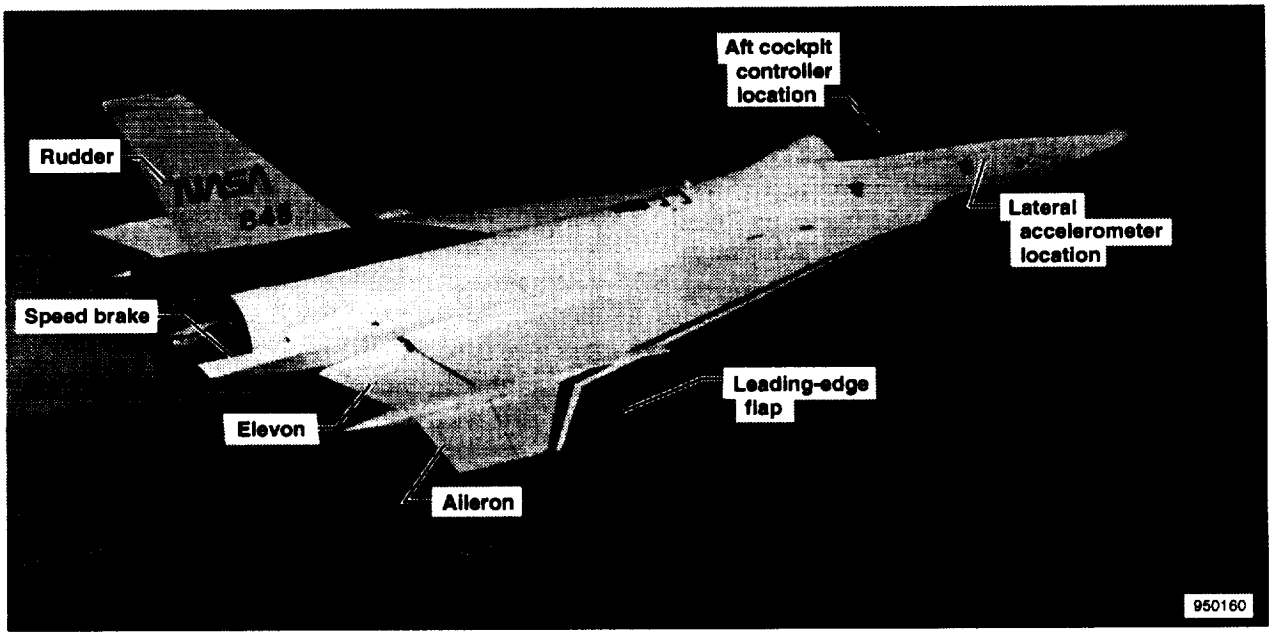

Figure 1. The F-16 XL-2 aircraft surfaces and pertinent control units.

of the primary and secondary control surfaces and relevant control system units. Table 1 shows the pertinent physical characteristics and geometry of the aircraft.

Flight Control Systems

The F-16 XL aircraft derives total vehicle control from aerodynamic surfaces. The surface positions depend on the primary control input and the feedback response as measured by the aircraft rate sensors.

Aerodynamic Surfaces

Flightpath control, in both pitch and roll, is achieved by a blend of the aileron and elevon surfaces. The surfaces are faired along the trailing-edge segments of the

Table 1. The F-16 XL-2 physical and geometric characteristics (ref. 3).

Wing	
Area, ft^2	663.259
Span (theo.), in.	388.84
Aspect ratio	1.583
Taper ratio	0.128
Leading-edge sweep	
Inboard	70°
Outboard	50°
Incidence	–0.65° at BL 41.50, –4.104° at 136.1 and tip
Dihedral	0°
Mean aerodynamic chord, ($\bar{c}$) ft	24.7
Elevon area, ft^2	44.055
Aileron area, ft^2	29.445
Leading edge flap Area, ft^2	18.197
Vertical tail	
Area, ft	54.75
Span, in.	101.00
Aspect ratio	1.294
Taper ratio	0.437
Leading-edge sweep	44.5°
Bicon airfoil, percent	
Root	5.3
Tip	3.0
Rudder area, ft^2	11.65
Speed brake area, ft^2	14.26
Control-surface authority (normal to HL)	
Elevons	30° up, and down
Ailerons	20° up, 30° down
Leading-edge flaps	6.4° up, 36.5° down
Rudder	30° left and right
Speed brakes	60° up and down
Control-surface rates, deg/sec at zero load	
Elevons	60
Ailerons	60
Leading-edge flaps	31
Rudder	90
Speed brakes, per panel	30
Pertinent physical locations cg ~ 45%	*FS* 324
Lateral acceleration sensor	*FS* 118
Aft cockpit controller	*FS* 162

wing. Directional control is accomplished by a conventional rudder mounted on the trailing edge of a single vertical stabilizer.

Fly-By-Wire and Primary Control

A full fly-by-wire analog system is used in all three axes. The system is fully quadruple-redundant. Electrical signals from the analog flight control computers go directly to the integrated servoactuators. These actuators provide the force and position for the primary control surfaces. The electromechanical actuators are single-fail-operate components.

Secondary Systems

Leading-edge flaps (LEFs) are located outboard on the cranked portion of the wing. The LEFs are scheduled to operate symmetrically as a function of angle of attack and Mach number. Limited LEF differential trim input is available in conjunction with the normal aileron roll trim:

$$\Delta\text{LEF (maximum)} = 3.0° \quad \text{for } q_c \geq 2176 \text{ lb/ft}^2 \tag{1}$$

The LEFs also provide partial spin recovery by operating differentially ($\Delta\text{LEF} \approx 40°$) for angles of attack greater than 35°.

Speed brakes are located on the aft portion of the fuselage inboard of the elevons and in the horizontal plane. The brakes operate by rotating into the vertical directions to provide deceleration and additional spin recovery capability.

Sidearm Controller and Augmentation

The F-16 XL airplane has the same two-axes minimum displacement sidearm controller used on production F-16 aircraft. Figure 2(a) shows the relative

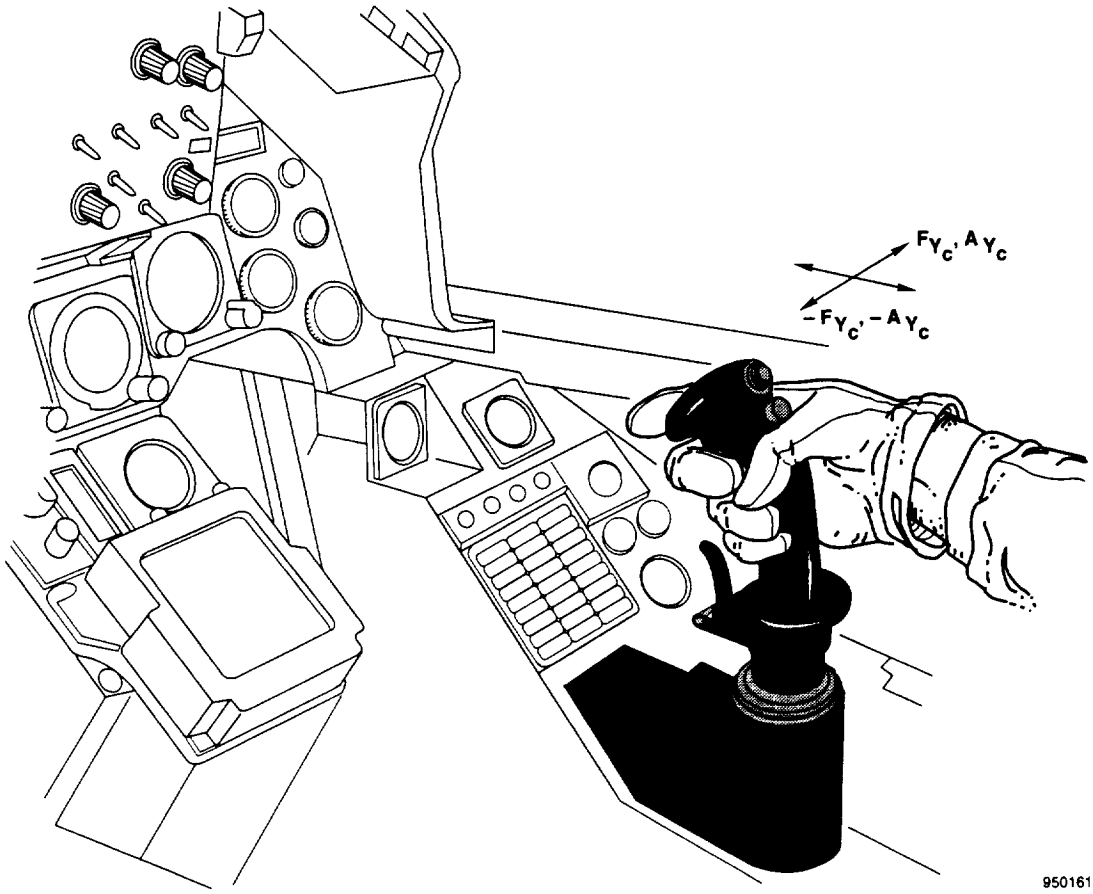

(a) Location of the pedestal-mounted controller within the cockpit.

Figure 2. Pitch and roll minimum displacement sidearm controller.

cockpit location and the size and shape of the controller. Figure 2(b) shows the wrist and elbow rests provided on F-16 aircraft. Use of the rests is optional; the rests can be stowed. Most pilots use only the elbow rest during rolling maneuvers.

By applying force to the controller, the pilot initiates pitch and roll inputs to a rate command augmentation system rather than to controlling surface positions directly. Longitudinal force input commands a blend of pitch rate and normal acceleration. The pitch feedback loops attempt to provide response characteristics invariant with flight conditions. Lateral force inputs command roll rate according to a roll command gradient schedule (fig. 3). The gradient consists of linear

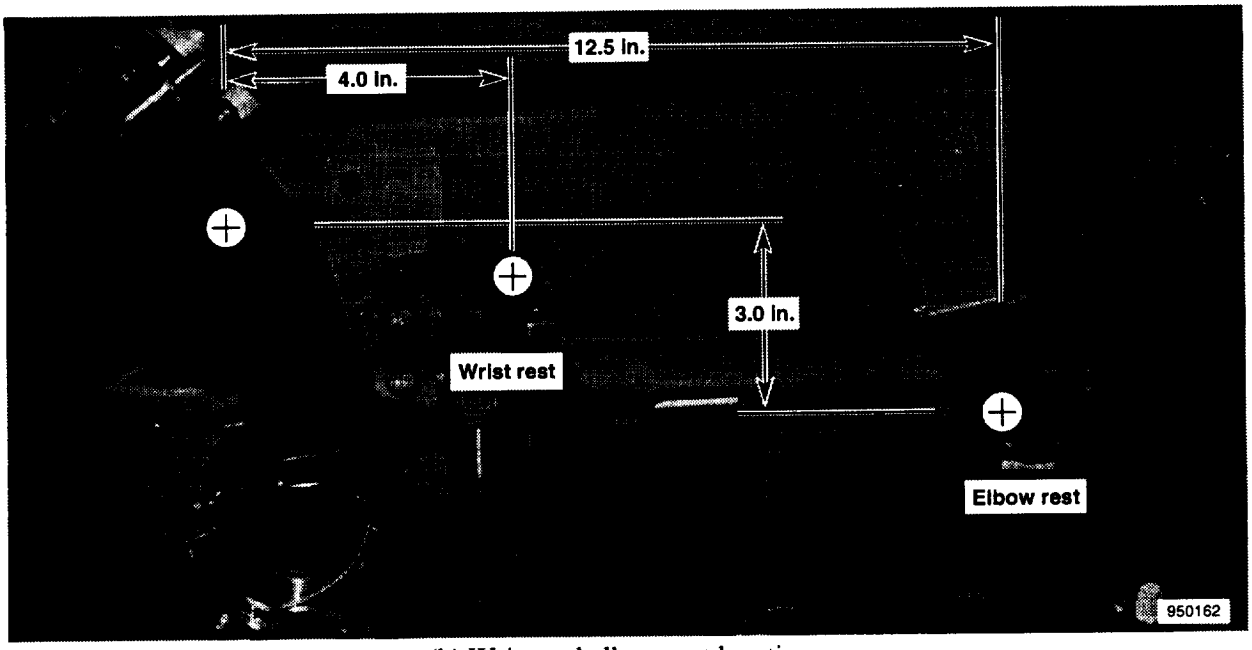

(b) Wrist and elbow rest locations.

Figure 2. Concluded.

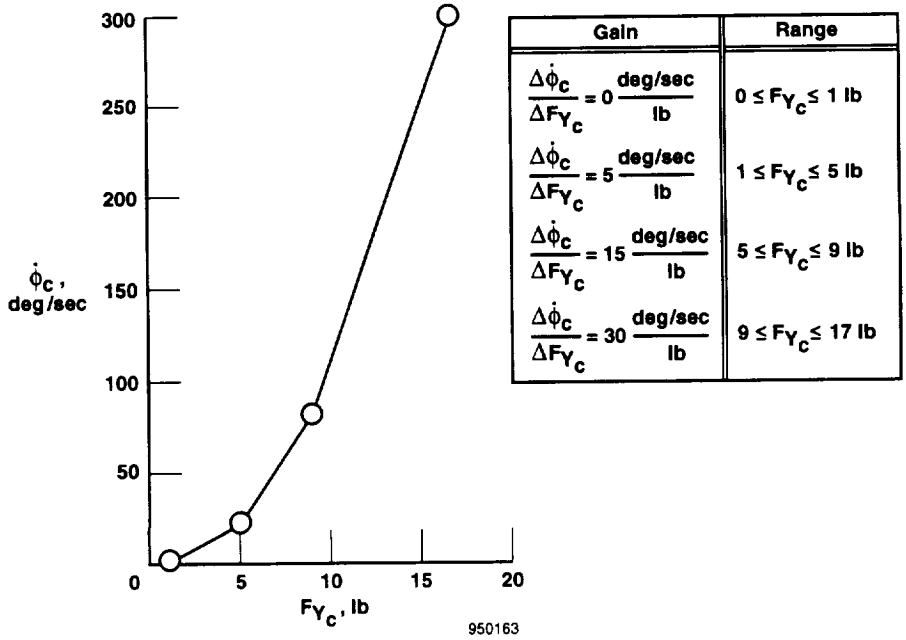

Figure 3. Roll command gradient and gain over the linear range.

constant rate gains/lb over the ranges shown with a maximum commanded roll rate of 300 deg/sec. A force input of 9 lb and larger produces a maximum gain of 30 (deg/sec)/lb. The force is actually determined by a transducer measuring displacement, $F_{Y_c} = F_{Y_c}(x_c)$. While force and displacement are well-correlated statically, the phase lag between applied force and resulting displacement is important in any transient analysis. A breakout force of ±1 lb is required for any transducer output, after which the transducer output is essentially linear up to a maximum displacement of 0.25 in. at 20 lb (a spring constant of 80 lb/in or 960 lb/ft). Total surface position command is proportional to the error signal, ε, as shown by the functional roll control system diagram (fig. 4). Favorable roll-yaw coordination is provided through a scheduled and function-generated aileron-rudder interconnect.

A typical rate damper stability augmentation system is implemented in the yaw axis to accomplish both dynamic and static stability. Aircraft dynamic stability is augmented by a washout yaw rate feedback. Static directional stability is augmented by lateral acceleration feedback.

A more complete and detailed description of the flight control, its design and final configuration philosophy, and the surface rates and authorities has previously been given.[13,16]

Instrumentation

The F-16 XL-2 instrumentation was designed, installed, and maintained by the NASA Dryden Flight Research Center. Most of the data originate from flight control sensors and are obtained from the avionics data bus. The data presented in this report were recorded from pulse-code-modulation telemetry. The aircraft rates, surface positions, and aircraft system functions were recorded at 50 samples/ sec. Tables 1 and 2 show flight control accelerometer locations.

FLIGHT TEST EXPERIENCE

Many modern fighter aircraft experience roll oscillations. The occurrences follow rapid rolling maneuvers, particularly those performed at high-dynamic pressures.

Roll Ratcheting

During F-16 XL-2 flight 12, which in part was a functional check flight, the copilot performed three fairly rapid 360° rolling maneuvers from the aft cockpit. The copilot reported severe roll ratcheting particularly at high commanded roll rates and in the recovery.

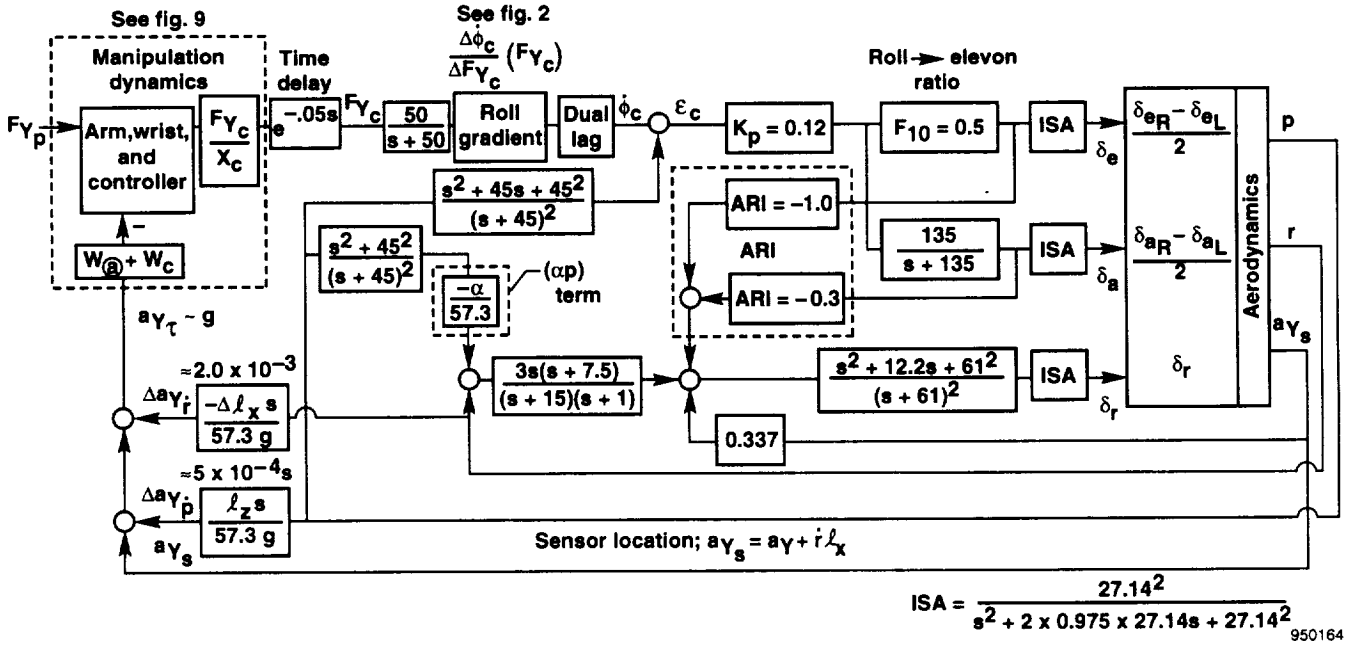

Figure 4. Basic F-16 XL function roll control system for the flight conditions listed in table 2.

Table 2 shows the flight conditions typical of all three maneuvers.

Table 2. Flight conditions, mass properties, and dimensions.

Mach number	0.9
Altitude, ft	11,600
Dynamic pressure, lb/ft^2	790
True airspeed, ft/sec	964
Angle of attack, deg	$1.77 < \alpha < 4.0°$
Angle of attack and pitch attitude, deg	3
Center of gravity, % $\bar{c}$	45
Weight, lb	28,318
Impact pressure, lb/ft^2	957.3
Impact pressure/static pressure	0.7
Vehicle moments of inertia, slug ft^2	
I_x	22,352
I_y	104,027
I_z	123,293
I_{xz}	–559
Longitudinal distance, ft (A/C accelerometer location, relative to *cg* and body axis)	17.0
Vertical distance, ft (A/C accelerometer location, relative to *cg* and body axis)	0.0
Controller location	
Longitudinal distance, ft	13.5
Vertical distance, ft	1.0

Figures 5 and 6 show time histories of the aircraft response and control parameters. Figure 5 shows the time response of the lateral controller force, bank angle, rolling angular rate, and lateral acceleration at the sensor for the three rolling maneuvers and recovery. The direction of the roll is indicated. Initially, the copilot banked right to approximately 60° and rapidly completed a full 360° roll to the left. The copilot continued the roll to the left at a slow rate and stabilized in a left-bank attitude for approximately 5 sec. From a wings-level attitude, the copilot completed another 360° left roll and stabilized the aircraft near 0° for approximately 10 sec before initiating a full 360° roll to the right.

At the recovery portion of all three rolling maneuvers, where $|F_{Y_c}(x_c)| > 9$ lb, the aircraft exhibited a considerable amount of roll ratcheting. The data show the oscillations are generally superimposed on a commanded and derived roll response. Consequently, for one-half cycle of each oscillation, the motion appears to the pilot as a periodic hesitation in the roll response. Thus, the terminology "roll ratcheting" is very descriptive of the phenomenon displayed.

Pilot Remarks and Comments

The copilot who performed the rolling maneuvers has a considerable amount of time and experience in flying F-16 aircraft. From a discussion with the copilot following the flight and a review of the flight data, the subsequent impressions were obtained, and the copilot's remarks and comments are summarized as follows.

The copilot was definitely aware of the ratcheting response. The copilot's primary attention was focused on the nose of the aircraft, so impressions were formed from the cyclic behavior and roll rate hesitation. The cockpit motion was of little concern during the occurrence. The copilot also thought that the body, torso, and shoulders were restrained sufficiently to be minimally responsive. The elbow rest was in use while the rolls were executed. The copilot felt the forces were low or unchanging at the arm during the ratcheting acceleration experienced. This observation and comment is understandable because the controller force transducer was responding to inertia forces of the arm and controller. The calculation of the controller displacement resulting from the observed variation in controller force supports this explanation. The minimum displacement controller has a stiffness defined by

$$F_{Y_c}(x_c) = 20 \text{ lb}; \; x_c = 0.25 \text{ in.} \tag{2}$$

The measured controller force variations (from figure 5(a)) are

$$\Delta F_{Y_c} = 2.5 \text{ lb peak-to-peak} \tag{3}$$

Then $\Delta x_c = (2.5/20) * 0.25 = 0.031$ in. peak-to-peak as indicated in the Aircraft and Controller Cycle Response section. This small controller displacement seems to explain the lack of pilot observation.

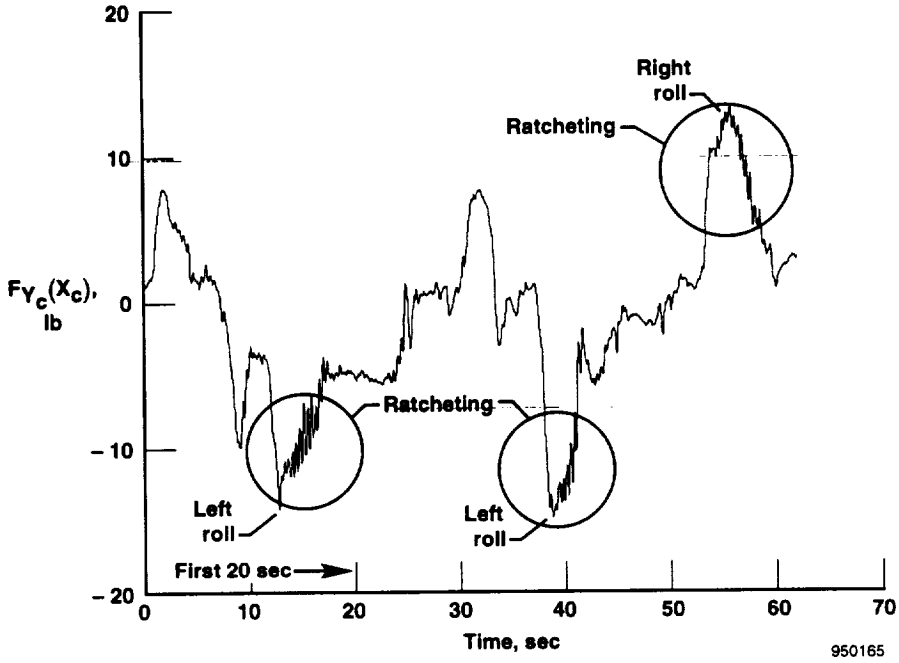

(a) Stick force (from the stick position transducer).

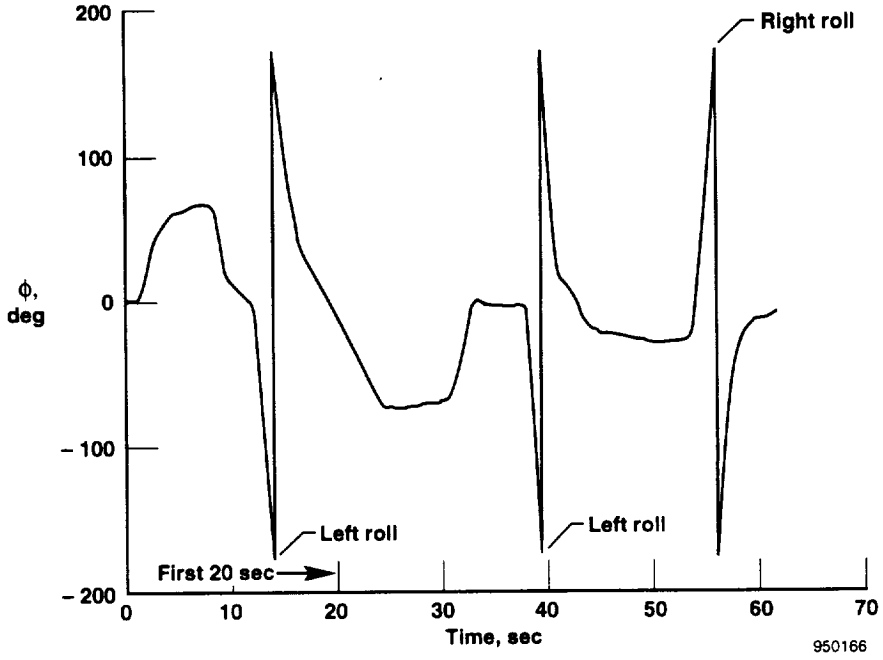

(b) Bank angle.

Figure 5. The F-16 XL-2 time histories during rolling maneuvers at the flight conditions listed in table 2.

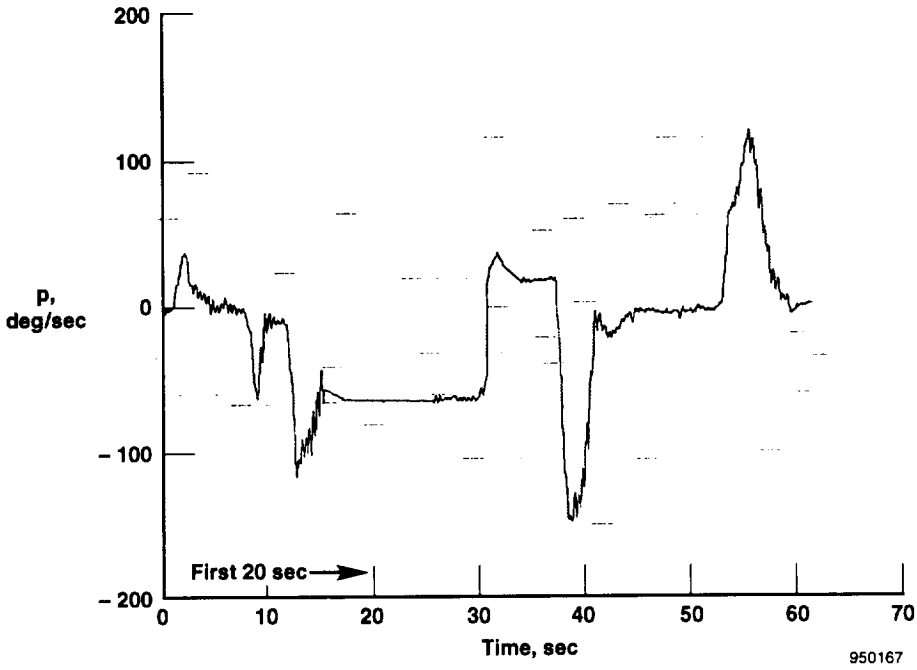

(c) Roll rate.

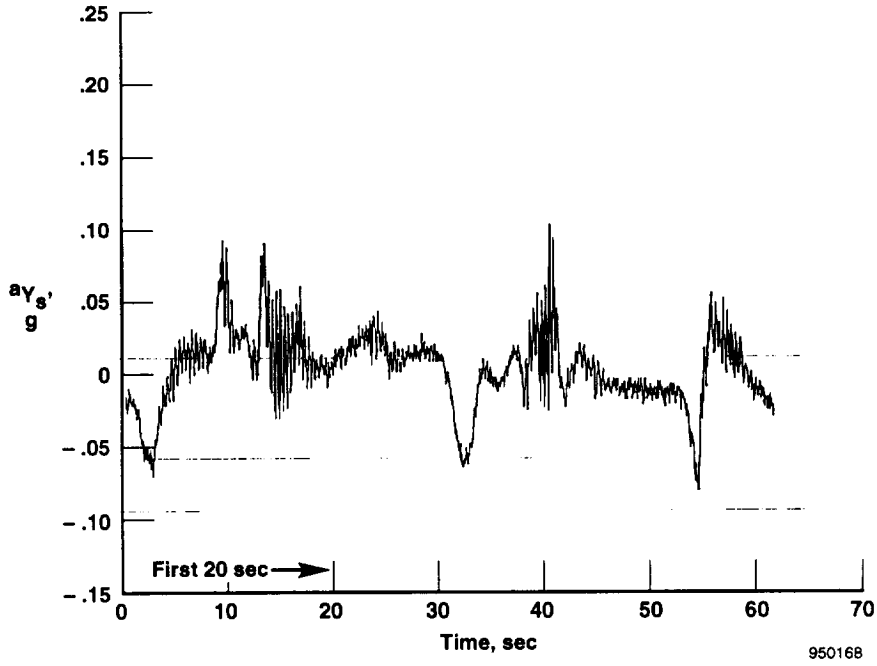

(d) Lateral acceleration (from the accelerometer in the front cockpit).

Figure 5. Concluded.

Aircraft and Controller Cyclic Response

By comparing the data from the three rolls (fig. 5), it is evident that the most extensive ratcheting occurred during recovery of the first rolling maneuver ($10 \leq t \leq 20$ sec). The discussion and analyses that follow consider the first rolling maneuver and recovery as distinctive representations of the displayed phenomenon.

Figure 6 shows time histories of the first 20 sec of the data shown in figure 5. These data present a complete 360° left rolling maneuver and recovery. All the aircraft response data relevant to the lateral control and the appropriate control surface positions are shown. The most interesting time span of the time histories exhibiting the roll ratcheting is from 13 to 17 sec. These data show the existence of 10 cycles of oscillatory motion lightly damped and at a frequency of 16 rad/sec or

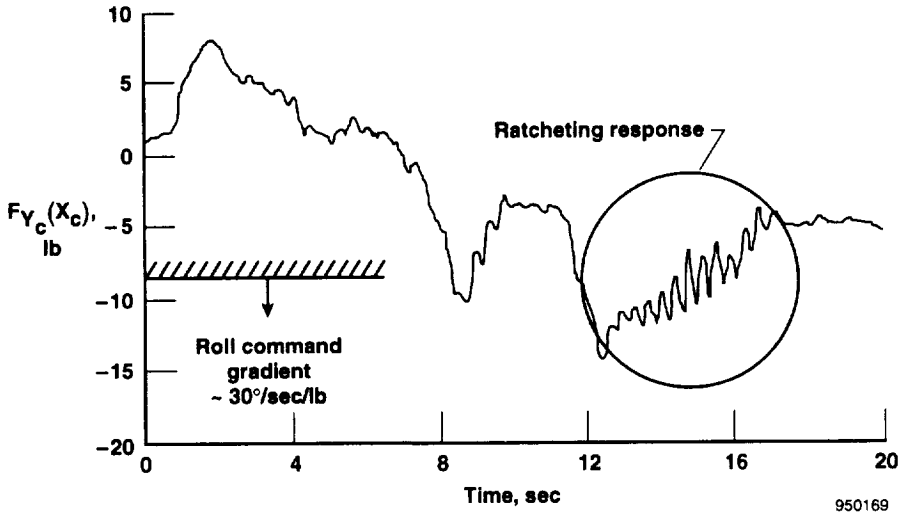

(a) Stick force (from the stick position transducer).

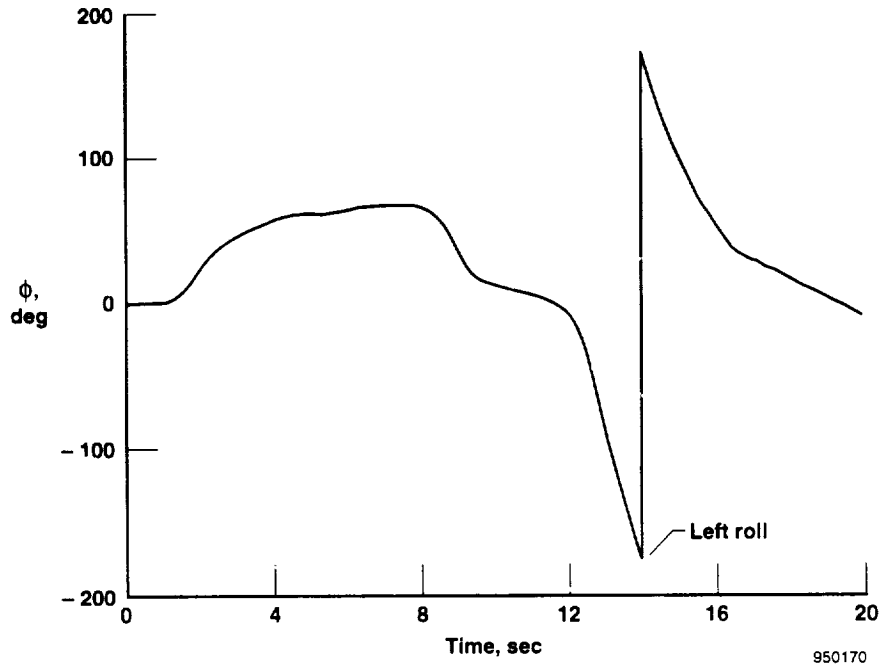

(b) Bank angle.

Figure 6. The F-16 XL-2 expanded time histories during rolling maneuvers at flight conditions listed in table 2.

approximately 2.5 Hz. This frequency falls within the range of frequencies considered typical of roll ratcheting as reported in various references.[1–3]

Note that the lateral controller force, which is a function of controller transducer output calibrated in lb, is very active during the roll ratcheting recovery (fig. 6(a)). This trace portrays a very lightly damped system oscillation and suggests that the controller is actually being excited through a "bobweight" effect that is sustained by lateral acceleration. At the initiation of the recovery, the force level $|F_{Y_c}|$ was greater than 9 lb. Figure 3 shows that the controller gradient doubles at a force level of 9 lb. The phenomenon observed is easily excited and sustained at high force levels. Fully saturated roll inputs ($|F_{Y_c}| > 17$ lb) would not provide a gradient gain for the feedthrough process. However, during a typical recovery from a saturated

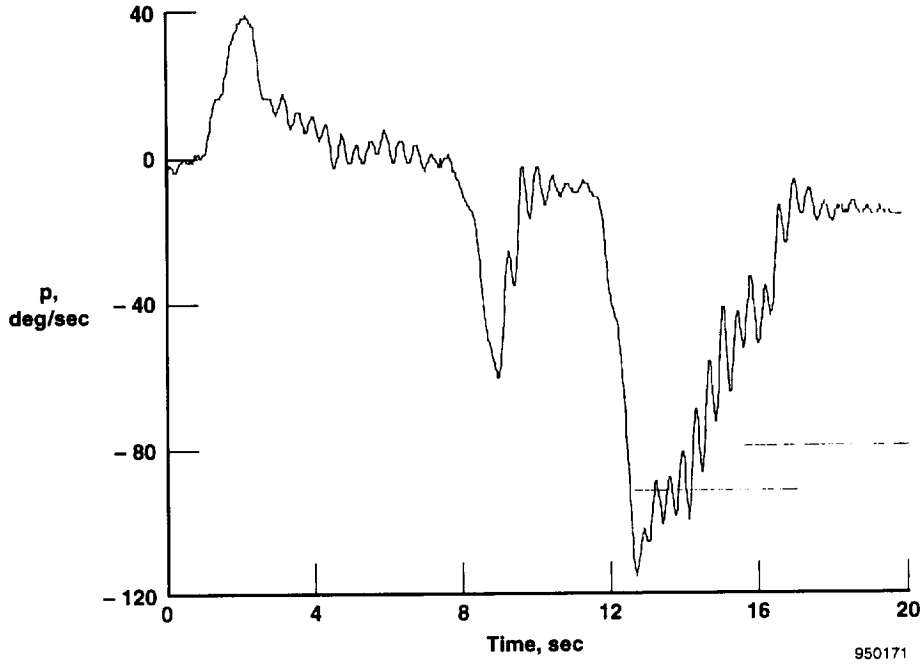

(c) Roll rate.

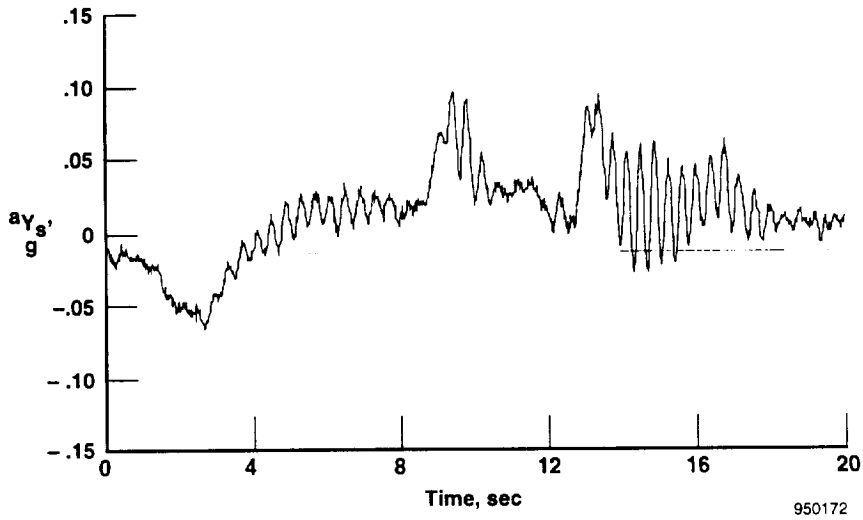

(d) Lateral acceleration (from the accelerometer in the front cockpit).

Figure 6. Continued.

condition, the roll ratcheting oscillations are likely to occur.

The time history data indicate a reduction in the oscillatory amplitudes as the controller force level decreases (fig. 6). The estimated peak-to-peak variations of the distinctive aircraft responses during the roll ratcheting segment are as follows:

$$\begin{aligned}
\text{Frequency range} &= 2.24\ \text{Hz} \le f \le 2.83\ \text{Hz} \\
&= 14 \le \omega \le 18\ \text{rad/sec} \\
\omega &= 16\ \text{rad/sec (average)} \\
\Delta a_{Y_s} &\approx 0.09\ g \\
\Delta p &\approx 21\ \text{deg/sec} \\
\Delta F_{Y_c}(x_c) &\approx 2.5\ \text{lb} \\
\Delta x_c &\approx 0.031\ \text{in.} \\
\Delta \dot{p} = \Delta p \omega &\approx 336\ \text{deg/sec}^2 \\
\Delta a_Y(\dot{p}) &\approx 0.18 g\ \text{(at the controller)}
\end{aligned}$$

The peak-to-peak roll response, $\Delta p = 21$ deg/sec, resulting from a controller force variation of $\Delta F_{Y_c}(x_c) = 2.5$ lb shows an amplitude of 8.4 (deg/sec)/lb for a frequency of 2.5 Hz. This change is approximately 28 percent of the commanded steady-state gain response (30 (deg/sec)/lb) for a controller force level of 9 lb and greater. The acceleration variation measured at the sensor indicates a maximum of $\Delta a_{Y_s} = 0.09\ g$. This variation gradually decreases after the first four cycles. Little, if any, response is evident in the yaw rate, r, time histories. All primary control surfaces exhibit the ratcheting oscillation. The rudder is particularly active and indicates a peak-to-peak displacement of more than 4° as a result of a_Y feedback.

Although the accelerations are vector quantities, a rough estimate of the pilot's arm weight can be obtained by adding the peak-to-peak magnitudes of the two components. This approach assumes that the arm can be modeled as a point mass at the controller (termed an equivalent weight).

$$\begin{aligned}
\Delta a_{Y_c} &= \Delta a_{Y_s} + \Delta \dot{p} \frac{l_z}{g\ 57.3};\ l_z \approx 1\ \text{ft} \\
&= 0.09 + 0.18 \\
&= 0.27\ g
\end{aligned} \tag{4}$$

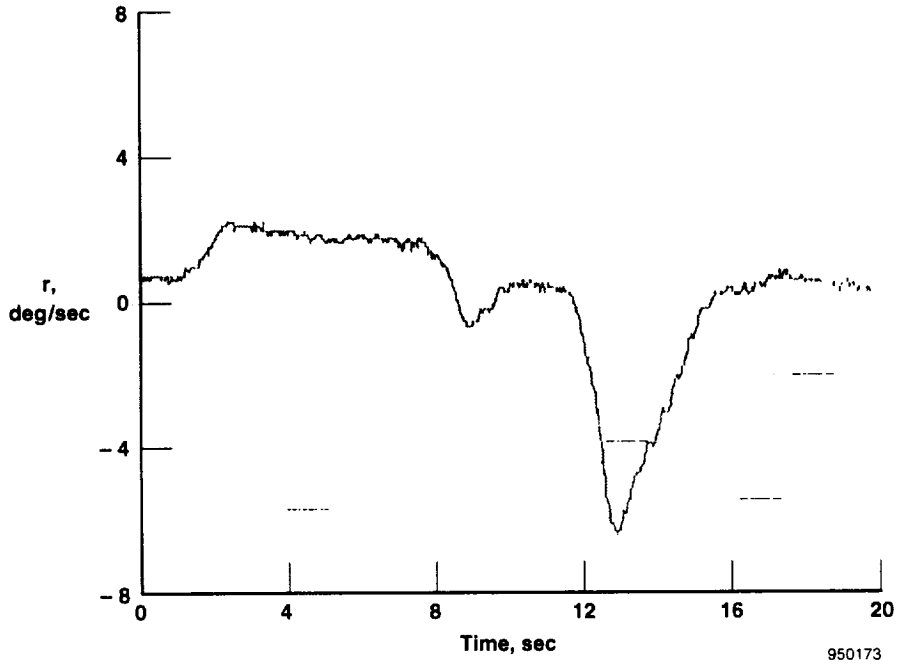

(e) Yaw rate.

Figure 6. Continued.

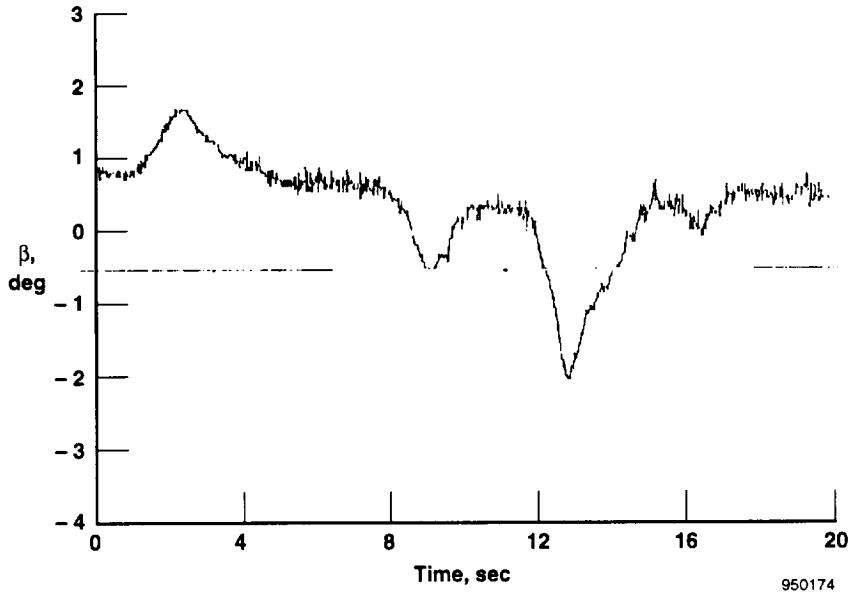

(f) Side slip.

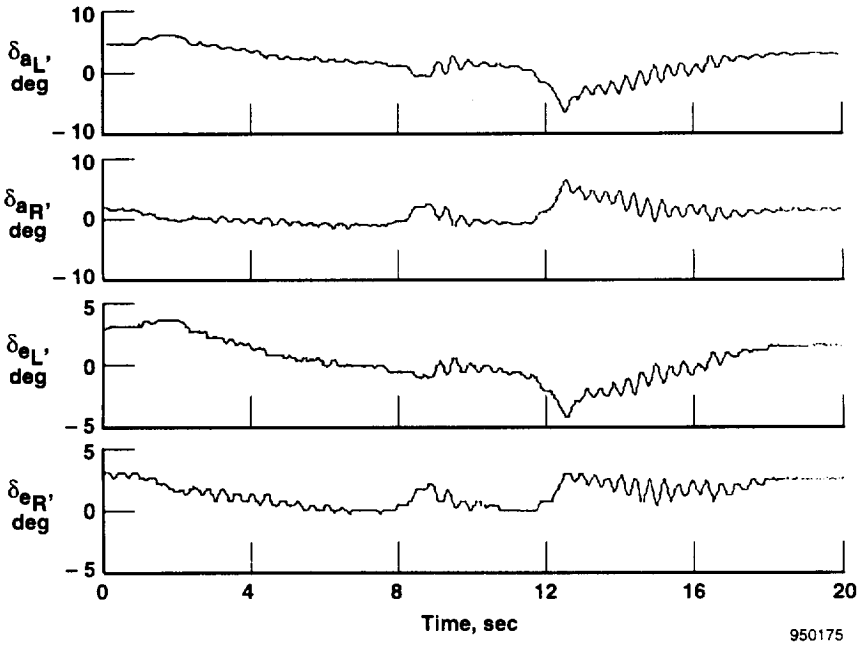

(g) Aileron and elevon positions.

Figure 6. Continued.

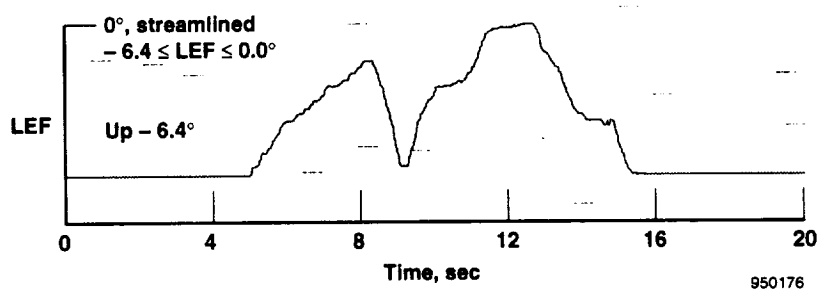

(h) Leading-edge flap position.

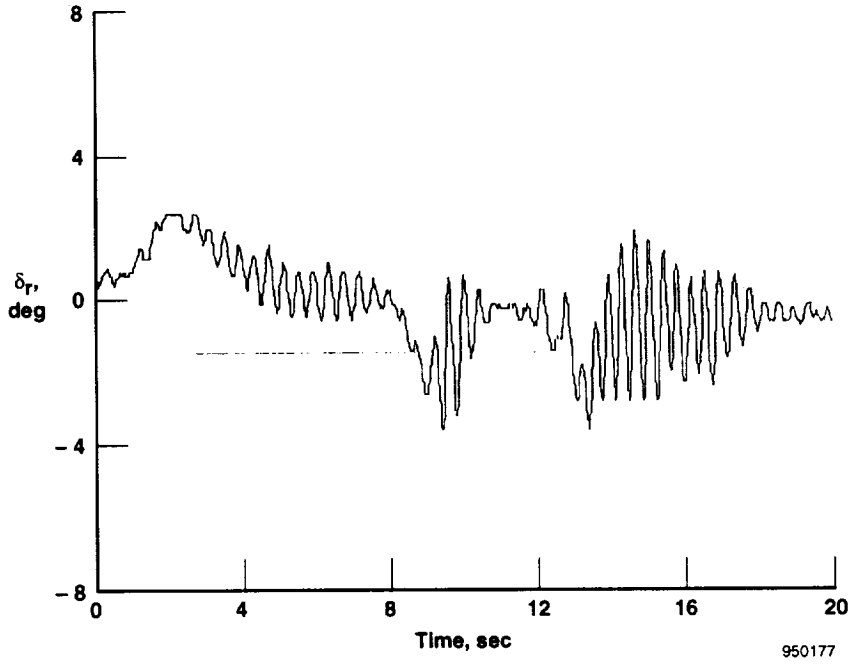

(i) Rudder position.

Figure 6. Concluded.

because

$$\Delta F_{Y_c} = 2.5 \text{ lb} \tag{5}$$

then

$$W_T(e) = \frac{\Delta F_{Y_c}}{\Delta a_{Y_c}} = 9.3 \text{ lb} \tag{6}$$

In modeling the pilot's arm, wrist, and hand and the sidearm controller, rotational as well as translational elements exist. The model converts the rotational elements into translational elements by defining equivalent weights that include moment of inertia terms. The equivalent weight of the arm, $W_{@}(e)$, is equal to the total equivalent weight of the arm and controller, $W_T(e)$, minus the weight of the controller, W_c. The controller weighs 1.25 lb.

$$\begin{aligned} W_{@}(e) &= W_T(e) - W_c = 9.30 - 1.25 \\ W_{@}(e) &= 8.05 \text{ lb} \end{aligned} \tag{7}$$

ANALYSIS AND DISCUSSION

Previous roll ratcheting investigations and analyses considered the pilot not only as a connective link but as an active element of the closed-loop process. The following discussion considers the pilot's role as the active controlling element. However, the major investigation and analysis focuses on the force feedthrough effect resulting from lateral acceleration and the partially restrained controller and arm masses.

Roll Ratcheting Investigation, Scope, and Definitions

Studies of roll ratcheting oscillations encountered by high performance aircraft have considered the pilot's role in a closed-loop process.[4, 5] The biomechanical feedthrough effect caused by the product of the lateral acceleration and the sum of the arm and controller masses have also been studied.[10]

Figure 7 shows two simplified illustrations depicting the control process in deriving a roll rate, capturing a roll attitude, or maintaining a bank angle. Figure 7(a) shows a simulated forcing function. The pilot, while continuously observing the desired error signal, actively tries to minimize the signal. How well the task is accomplished becomes a qualitative assessment and may be quantized as indicated for a comparison with another test configuration. The variables in most cases are the pilot or operator, the controller, and the controlled element. Analytically, the operator is modeled by a transfer function composed of a gain constant, a time delay, and some form of equalization. The controller is represented by its dynamic response characteristics. The controlled element is defined by the aircraft transfer functions.

Figure 7(a) depicts a task system of an in-flight investigation using a T-33 variable stability aircraft[4, 5] exemplifying the study of the pilot's role. During tracking tasks, the investigators varied such parameters as time delays, prefilter lag-lead models, and augmented roll mode damping. One reported finding was that roll ratcheting tendencies increase with augmented roll damping and the subsequent oscillations resulted in poor pilot ratings. This finding is logically consistent with the conclusions of this report. Increasing the augmented roll damping, decreases steady-state roll rate response to a pilot input. Large pilot inputs or a high gain on the pilot input are, therefore, required to minimize the error signal, which is a function of roll rate

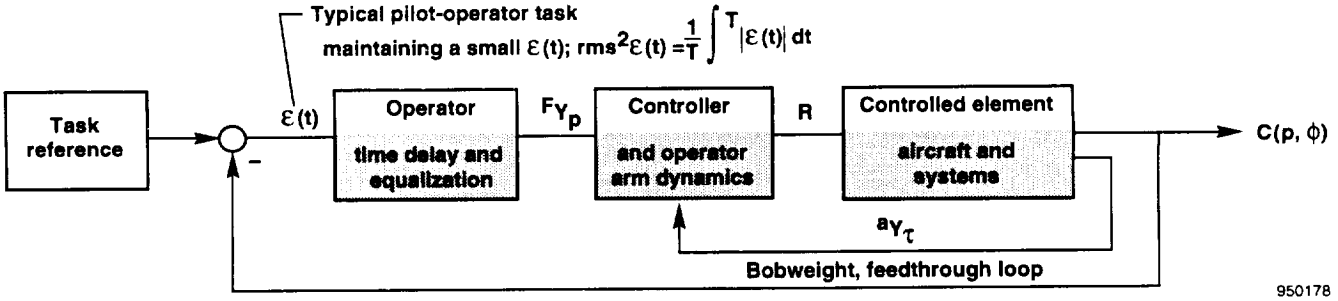

(a) System with a forcing function or task reference; operator controlling to minimize an error signal.

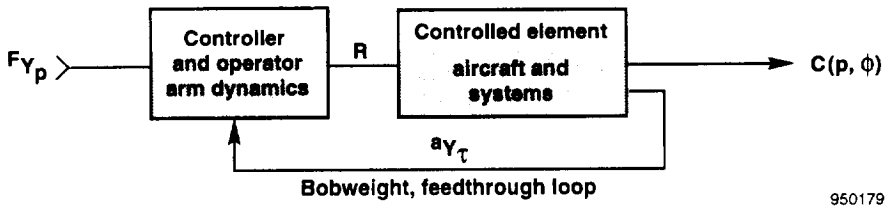

(b) System to achieve desired roll rate and roll attitude.

Figure 7. Basic human operator system concepts for acquiring a prescribed task.

and bank angle. The large inputs result in large initial roll and lateral acceleration responses, which lead to an increase in roll ratcheting oscillations. Large inputs also result in increased stick gain (via nonlinear stick gearing). Such gains also lead to an increase in roll ratcheting susceptibility.

The present investigation simply considers the pilot performing in-flight rolling maneuvers with no minimization task required. Figure 7(b) shows this control process. First, the pilot applies a roll control force to the controller, F_{Y_p}, to achieve the desired roll rate. Then, the force is decreased or reversed near the desired roll attitude. Rolling the aircraft generates tangential acceleration components at the controller composed of, $l_x\dot{r}$, $l_z\dot{p}$ and aircraft lateral acceleration, a_Y. The product of the equivalent weight and sum of the accelerations causes an additional force input, ΔF, that is superimposed on the reference force input, $(F_{Y_p} + \Delta F)$. This reaction results in a closed-loop feedthrough effect that produces an overall reduction in gain margin. This closed-loop process is generally referred to as a "bobweight" effect.

Assuming the arm is modeled as a cylinder with uniform mass distribution rotated about an endpoint, then the equivalent weight of the arm at the controller is equal to one-half the weight of the arm, $W_@$, plus the moment of inertia effect. The moment of inertia effect is $W_@/3$.

$$W_@(e) = \frac{W_@}{2} + 0.33\,W_@ \tag{8}$$

Using the equivalent weight of the arm as estimated in equation 7 from the flight data, then

$$\begin{aligned} 8.05 &= 0.83 W_@ \\ W_@ &= 9.7 \text{ lb} \end{aligned} \tag{9}$$

If the elbow rest completely immobilized the upper arm, then the equivalent weight would be determined from the forearm and hand. The flight-determined arm weight of 9.7 lb appears to be approximately twice the expected weight for forearm and hand (approximately 5 lb). Apparently, the elbow rest was only partially effective in restricting the motions of the upper arm.

The total body weights of four cadavers and the weights of body components including arm segments have previously been given.[17] The arm component weights for a 165-lb adult male cadaver, expressed as a percentage of total body weight, are as follows:

Entire arm	6.59 percent
Upper arm	3.44 percent
Forearm and hand	3.15 percent
Forearm	2.26 percent
Hand	0.89 percent

Based on the F-16 XL pilot's weight, 160 lb, the comparable arm components weights are estimated to be

Entire arm	10.54 lb
Upper arm	5.50 lb
Forearm and hand	5.04 lb
Forearm	3.62 lb
Hand	1.42 lb

Assuming that the elbow rest was ineffective during the oscillations, then the equivalent weight at the controller would be determined from the weight of the entire arm ($W_@ = 10.54$) as follows:

$$\begin{aligned} W_@(e) &= \frac{W_@}{2} + 0.33 W_@ \\ &= \frac{10.54}{2} + 0.33*(10.54) \\ W_@(e) &= 8.75 \text{ lb} \end{aligned} \tag{10}$$

Subsequent analytical calculations vary the equivalent weight of the entire arm arbitrarily between the two extremes $(3.93 \le W_@(e) \le 10.75)$.

Integrated Modeling Description

Figure 4 shows a functional block diagram of the F-16 XL roll control system. Pilot input, F_{Y_p}, is indicated as the reference input to the controller. A force input initiates the roll command through the force and roll gradient and is summed with the augmentation roll rate feedback. The result generates a roll response through the plant aerodynamics that is proportional to the error signal. Figure 4 shows the aileron-to-rudder interconnect and the angle of attack and roll rate (αp

term) configurations on the F-16 XL airplane. The input/output relationships for the plant aerodynamics are described in appendix B. Lateral–tangential accelerations at the controller are generated because of the roll response and the additional lateral degrees of freedom. These accelerations are computed in g. Along with the respective equivalent weights of the controller and pilot's arm, these accelerations provide a force-feedthrough process back into and through the controller. The dynamic response of the controller was determined from release tests with various weights added. The results are presented in appendix C. The natural frequency of the controller is well-separated from the ratcheting frequency. Consequently, the controller dynamics have a small effect on the ratcheting response. The response of the controller at the ratcheting frequency can be determined by the second-order response curves found in any dynamics text. For $\omega/\omega_n \leq 0.3$ and $\zeta = 0.05$, the gain is approximately 1.0.

The manipulation dynamics are shown in the biomechanical feedthrough model (fig. 8). This particular illustration was adapted from a description previously given.[10] An extensive amount of experimental and analytical research regarding the biomechanical forces derived from accelerations was conducted.[10] This report relies heavily on those efforts and measurements. The complete formulation of the second-order systems and equation characteristics are derived in appendix D.

Figure 9 shows a mathematical model of the biomechanical nature of an operator's arm and wrist and the controller. The spring constant, damping coefficient, and time constants assigned to the respective second-order system equations were derived from the vibration platform and experimental tests previously performed.[10] By letting $s \rightarrow 0$, the steady-state gains become

$$\begin{aligned} \frac{K_i}{K_@ + K_i} &= 0.72 \\ \frac{K_@}{K_@ + K_i} &= 0.28 \end{aligned} \tag{11}$$

or the total steady-state force to the roll command gradient is

$$\lim_{s \rightarrow 0} F_{Y_c} = 0.72\left(F_{Y_P} - W_@(e)a_{Y_\tau}\right) - W_c a_{Y_\tau} \tag{12}$$

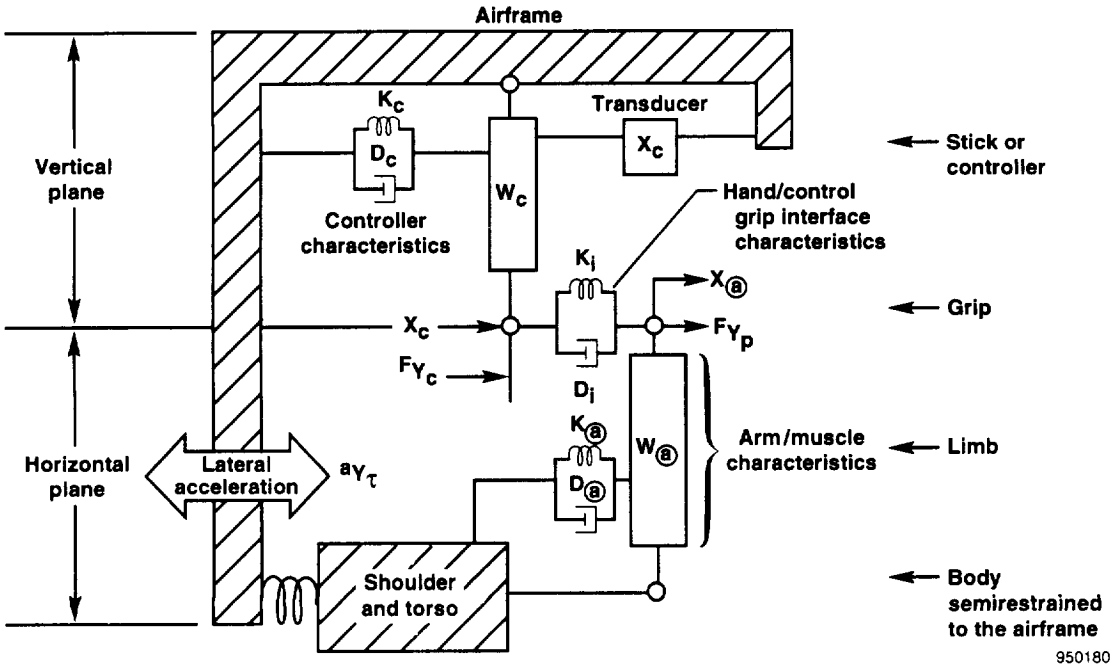

Figure 8. Feedthrough mechanical controller model with lateral force and acceleration input.[10]

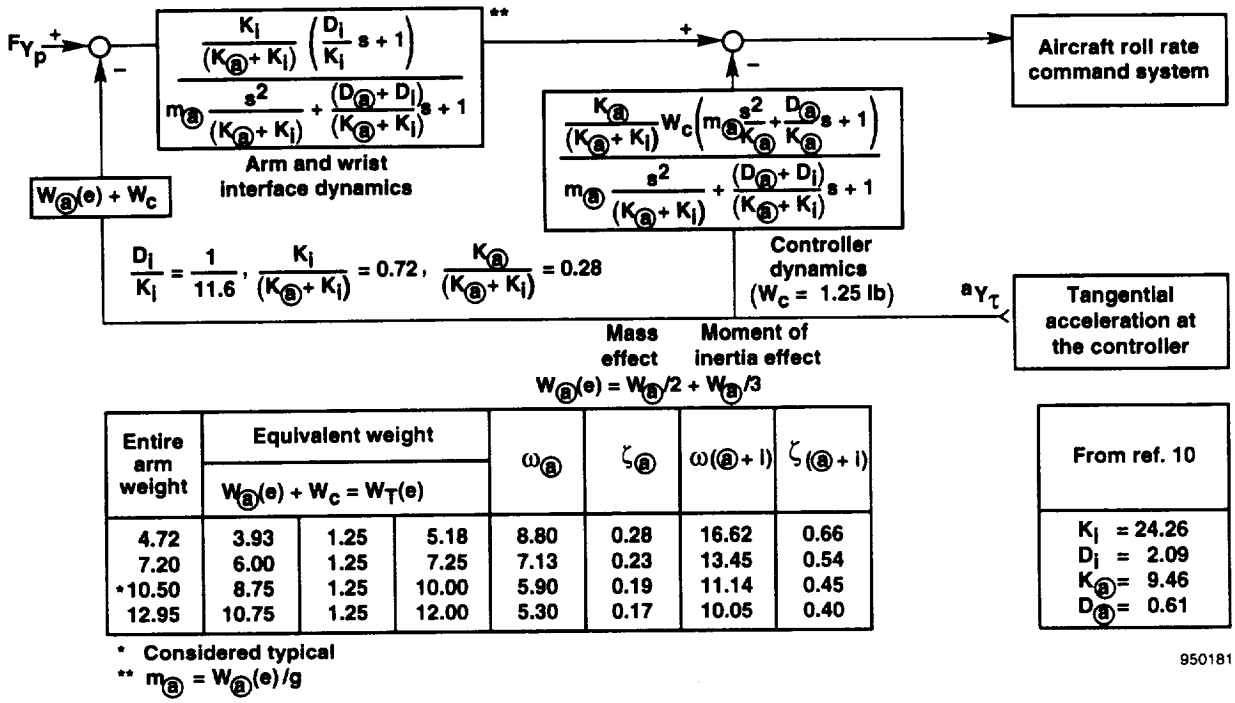

Entire arm weight	Equivalent weight $W_{(a)}(e) + W_c = W_T(e)$			$\omega_{(a)}$	$\zeta_{(a)}$	$\omega_{(a+I)}$	$\zeta_{(a+I)}$
4.72	3.93	1.25	5.18	8.80	0.28	16.62	0.66
7.20	6.00	1.25	7.25	7.13	0.23	13.45	0.54
*10.50	8.75	1.25	10.00	5.90	0.19	11.14	0.45
12.95	10.75	1.25	12.00	5.30	0.17	10.05	0.40

From ref. 10

K_I = 24.26
D_I = 2.09
$K_{(a)}$ = 9.46
$D_{(a)}$ = 0.61

* Considered typical
** $m_{(a)} = W_{(a)}(e)/g$

950181

Figure 9. Biomechanical model and mathematical description of the operator's arm and controller dynamics (appendix D). The controller spring gradient, $K_c \ldots$, cancels out.

If the operator's hand is removed from the controller, then F_{Y_p}, K_i, and $D_i = 0$. Expectantly, this leaves the controller weight, W_c, as the only force feedthrough loop into the aircraft roll command system. However because $F_{Y_p} = 0$, the roll command gradient gain is very small (fig. 3). Consequently, little, if any, feedthrough effect would excite the forward loop.

The equivalent weights (fig. 9) are considered representative and within the normal range of a typical arm and controller. The equivalent controller weight, W_c, is considered equal to the actual weight of the controller at the disconnect location. The equivalent weights are used instead of mass and inertia because the calculated or measured tangential acceleration at the controller are conveniently expressed in g units.

Mathematical Computations

The flight control system (fig. 4) was linearized about the same flight test conditions (table 2) as the aerodynamics for the plant. A unique nonlinear closed-loop system, called a dual lag, is implemented on the F-16 XL airplane. This system provides a different command response depending on initial input, control bias, and frequency. Consequently, the control bias must be considered when determining the input/output relationship. Appendix E shows the development of an averaged linear transfer function for a sinusoidal input at the flight-experienced roll rate condition.

$$\frac{CO}{RI} = \frac{10(s+40)}{(s+6)(s+67)} \tag{13}$$

The open- and closed-loop total system characteristics were determined by using a FORTRAN control program.[15] Figure 10 shows an open-loop frequency response of the tangential acceleration/command force, a_{Y_τ}/F_{Y_c}. For the observed in-flight ratcheting frequency, 16 rad/sec, the computed system shows a gain margin of 27 dB and a phase margin of 70°. At the crossover frequency, ω_{co} = 26 rad/sec, the gain margin is 35 dB. Note that a gain increase of 10 dB exists near the ratcheting frequency. This gain increase undoubtedly increases the tendency of the system toward instability when coupled with the manipulation dynamics.

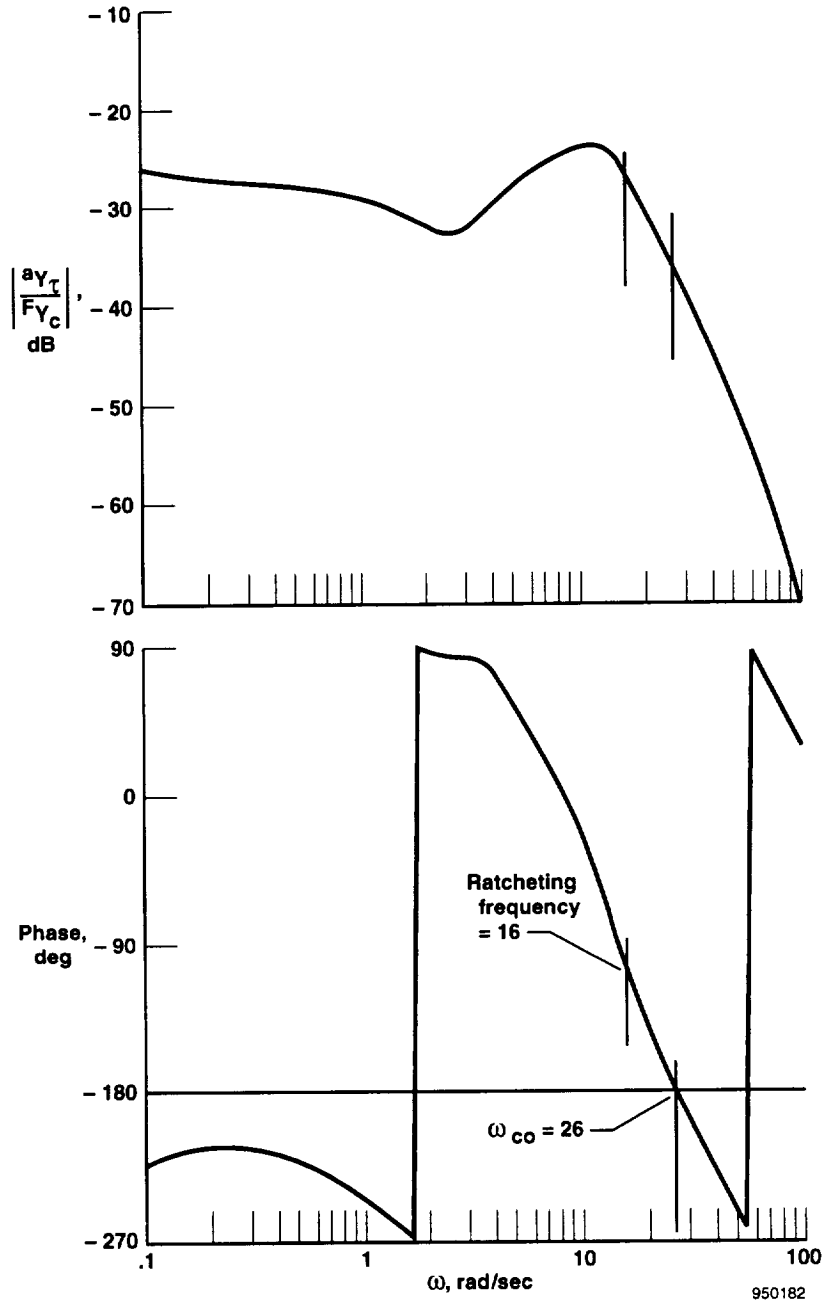

Figure 10. Open-loop tangential acceleration frequency response (conditions: $\dot{\phi}_c / F_{Y_c}$ = 30 (deg/sec)/lb. No manipulation dynamics or time delay at the flight conditions shown in table 2).

Figure 11 shows a comparison of the vector components of the tangential accelerations at the controller using the same open-loop computation (except ω = 15.6). The tangential accelerations are caused by roll acceleration, $\dot{p}$, and the lateral–translational acceleration, $a_Y + l_x\dot{r}$. Δa_{Y_τ} resulting from $\dot{p}$ lags the translational acceleration by approximately 180°, and the amplitude of the $\dot{p}$ vector is 2.17 times greater than the translational vector, $f(a_Y, \dot{r})$. The resultant vector is also shown and has a phase angle of –107° with a magnitude of 0.047 g.

Biodynamic Response

Figure 8 shows the arm, wrist interface, and controller feedthrough model. Manipulation dynamic characteristics are derived and developed in appendix D. Figure 9 shows the numerical values. The total system is thus described by inserting the manipulation transfer functions into the aircraft and functional control system diagram (fig. 4). Using this completely integrated model and applying the mathematical control program connective procedures,[15] the dynamic characteristics and time responses of the total system were obtained.

Figure 12 shows the open-loop frequency responses for four equivalent total weight conditions: $W_T(e)$ = 5.18, 7.25, 10.00, and 12.00 lb. For $W_T(e)$ = 5.18 lb, the open-loop system indicates a sufficient gain margin of 15 dB at ω_{co} = 20 rad/sec. Progressively increasing the equivalent total weight decreases the crossover frequency and decreases the gain margin. At an equivalent total weight of 12 lb, the system becomes very lightly damped at a frequency of approximately 10 rad/sec. A nominal and perhaps typical value for an equivalent total weight is believed to be approximately 10.0 lb, which means that the equivalent arm weight about the shoulder is as follows:

$$W_{@}(e) = W_T(e) - W_c = 8.75 \text{ lb} \tag{14}$$

The equivalent weight includes a moment of inertia effect;

$$W_{@}(e) = W_{@} \text{ (entire arm)/2} + 0.33 W_{@} \text{ (moment of interia)} = 0.8 \text{ lb} \tag{15}$$

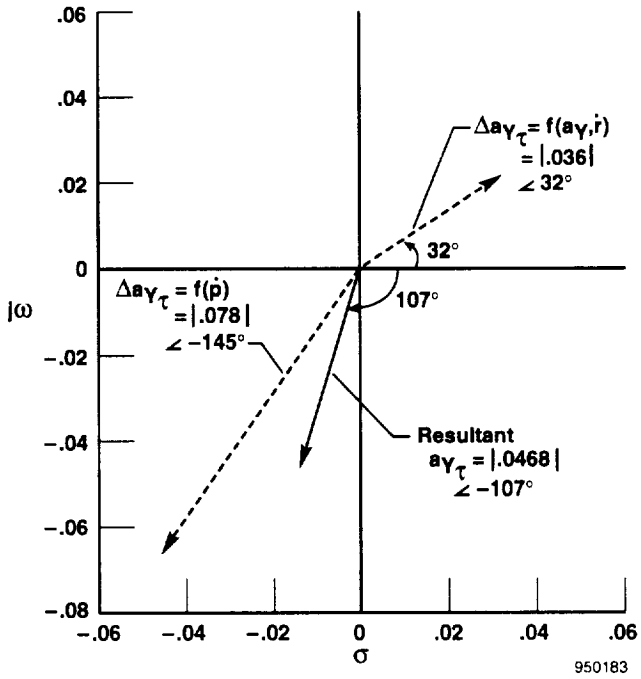

Figure 11. Open-loop vector components of the resultant tangential acceleration at the controller ($\dot{\phi}_c / F_{Y_c}$ = 30 (deg/sec)/lb; ω = 15.6 rad/sec. No manipulation dynamics or time delay at the flight conditions shown in table 2).

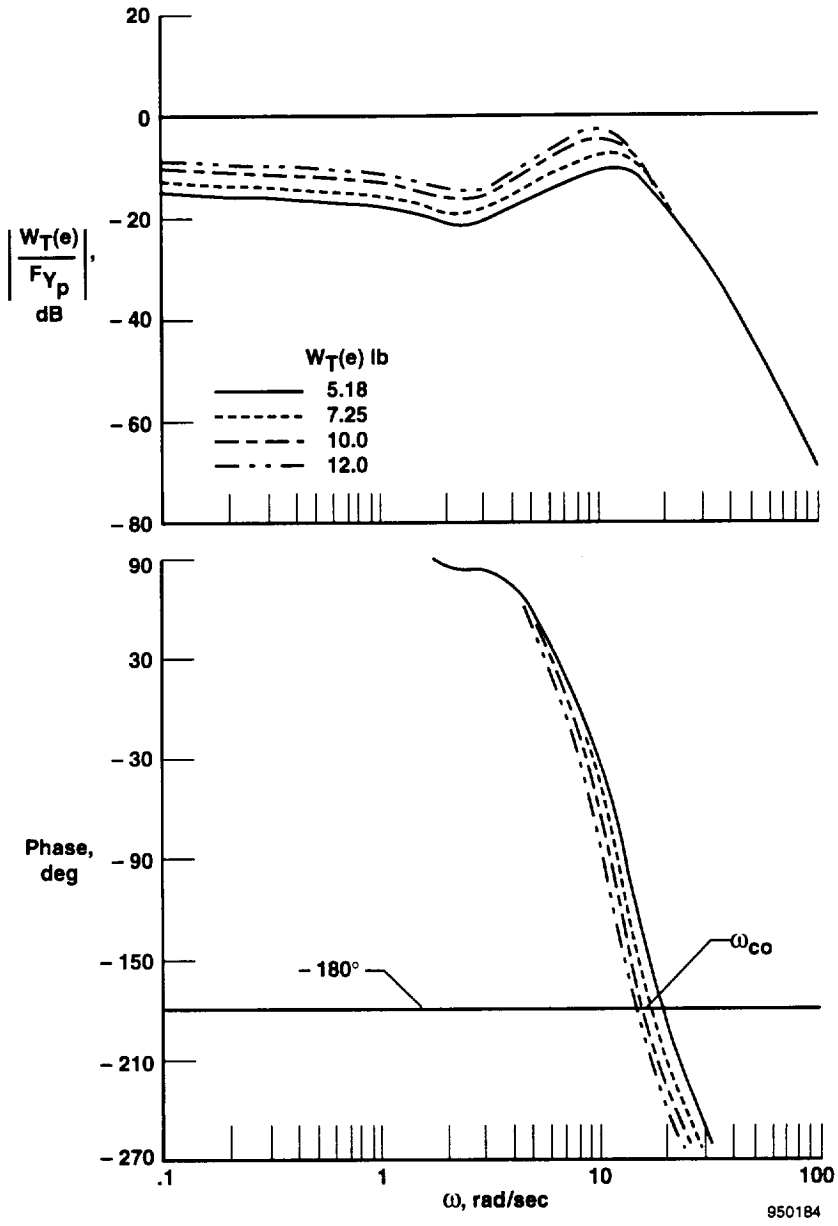

Figure 12. Open-loop frequency response as a function of total equivalent weight (fig. 9) (conditions: manipulation dynamics with no time delay at the flight conditions shown in table 2).

or the actual weight of the entire arm is

$$W_{@} = 10.5 \text{ lb} \tag{16}$$

An arm weight of 10.5 lb is believed to approximate the pilot's arm weight and yet be conservative enough to provide sufficient damping.

Figure 13 shows a computed time history for a 1-lb step input at F_{Y_p}. Eigenvalues show the mode to have a natural frequency of 14.3 rad/sec and a damping ratio of 0.15. This frequency is within the range observed from the flight data. To determine the effects of time delays, 50 msec of delay was added in the forward loop of the system (fig. 4). This delay changed the natural frequency and damping ratio to $\omega_n = 13.2$ rad/sec and $\zeta = 0.10$.

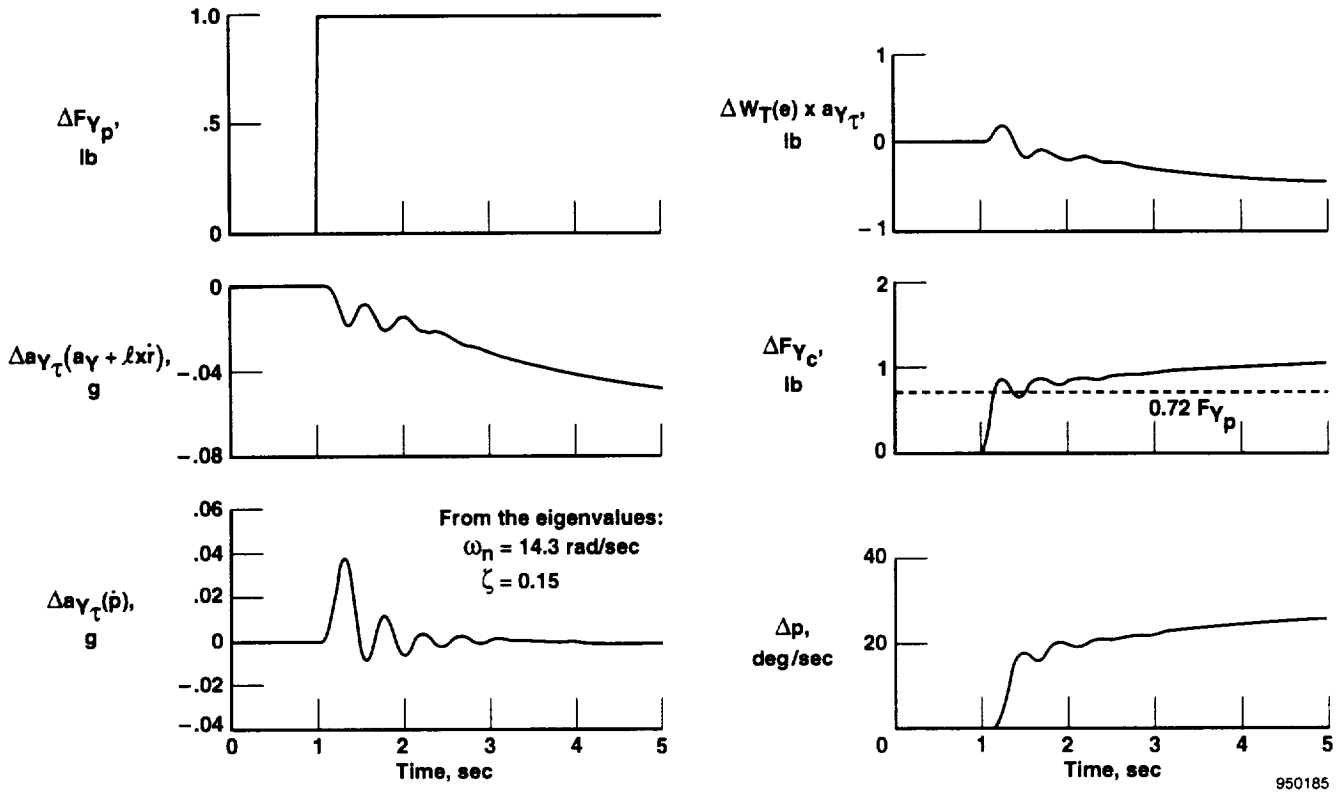

Figure 13. Analytically obtained time history in response to a unit step input (conditions: $W_T(e)$ = 10 lb, $\dot{\phi}_c / F_{Y_c}$ = 30 (deg/sec)/lb, no time delay, at the flight conditions of table 2).

CONCLUSIONS

The F-16 XL-2 airplane is a modified version of the production F-16 aircraft. Modifications include extending the forward and midfuselage by 56 in. and changing the wing to an advanced cranked arrow type. In place of horizontal tails, the F-16 XL-2 airplane derives total pitch and roll control by elevons and ailerons mounted along the trailing edge and throughout the span of the wing. The aircraft has a fly-by-wire analog flight control system approximately identical to the early F-16 aircraft. A minimum-displacement, two-axes, sidearm controller is used to command the pitch and roll rates.

During a functional check flight, the copilot, flying in the aft seat, completed three rapid rolling maneuvers. Upon recovery from each maneuver, the copilot reported roll ratcheting oscillations that lasted through 10 cycles at a frequency of 2.5 Hz. The roll command gradient gain was at its maximum of 30 (deg/sec)/lb initially and remained near the maximum throughout the oscillations.

The following conclusions were reached from flight test results and the analytical studies regarding the phenomenon:

1. During the roll oscillations, the controller transducer showed oscillations of the same extent, phase, and continuation as other aircraft roll response parameters. The data support the hypothesis that the oscillations were commanded through the controller.
2. Based on the controller force data, the maximum peak-to-peak controller displacement during the roll ratcheting oscillations was very small, $\Delta x_c \leq$ 0.032 in. This displacement indicates small arm motions. The copilot observed no arm forces or motions and believed that there were none.
3. All primary control surfaces followed the roll ratcheting oscillations induced by tangential accelerations at the controller.

4. The open-loop, computed tangential response of the basic aircraft, a_{Y_τ}/F_{Y_c}, shows about 10 dB of gain increase near the roll ratcheting frequency. Coupling with the manipulation dynamics causes the closed-loop system to be prone to ratcheting instability.
5. The tangential component of the acceleration at the controller caused by rolling acceleration, $l_z\dot{p}$, is approximately 2.2 times larger than the component caused by aircraft lateral acceleration, $a_Y + l_x\dot{r}$. This observation indicates that roll ratcheting depends largely on $\dot{p}$ and on the distance of the controller above the roll axis.
6. The dynamic characteristics of the controller have only a slight effect on roll ratcheting. The ratcheting frequency is well-separated from the natural frequency of the controller determined in appendix C.
7. Both crossover frequency and gain margin decrease when equivalent arm weight, $W_{@}(e)$, increases.
8. Based on estimates from one in-flight rolling maneuver, the wrist and elbow rests appear to be ineffective in restraining the arm from the small motions associated with roll ratcheting. The estimate of equivalent arm weight based on flight data more nearly matches the weight of the whole arm than just the forearm and hand.
9. Following a step input of F_{Y_P} = 1 lb with a roll command gradient gain of 30 (deg/sec)/lb and an entire arm weight of 10.5 lb, the integrated system exhibits a slightly damped oscillation: ζ = 0.15 at a natural frequency of 14.3 rad/sec.
10. Adding a time delay of 0.05 sec in the forward loop decreased the damping and frequency to ζ = 0.10 and ω_n = 13.2 rad/sec.
11. A technique for predicting roll ratcheting has been developed. The method requires an augmented aircraft model, the derived aircraft accelerations at the controller, and the pilot arm weight. The method and equations can be applied to other aircraft and included in simulation studies.

Dryden Flight Research Center
National Aeronautics and Space Administration
Edwards, California, October 28, 1994

APPENDIX A
NOMENCLATURE

Abbreviations

ARI	aileron-to-rudder interconnect
FS	fuselage station, in.
GE	General Electric
ISA	integrated servo actuator
LEF	leading-edge flap
PIO	pilot-induced oscillation
TF	transfer function
XL	extra-long

Symbols

A	matrix coefficient, $(A' = C^{-1}A)$
a_Y	lateral acceleration at the center of gravity, g
a_{Y_c}	lateral acceleration at the controller, g
a_{Y_s}	lateral acceleration at the sensor, g
a_{Y_τ}	tangential acceleration at the controller, g
B	matrix coefficient, $(B' = C^{-1}B)$
b	reference span, ft
C	matrix coefficient
C_l	rolling-moment coefficient, rolling moment/qsb
C_{l_p}	roll-damping derivative, $C_l/\partial(pb/(2V))$, rad^{-1}
C_{l_r}	rolling moment due to yaw rate, $\partial C_l/\partial(rb/2V)$, rad^{-1}
C_{l_β}	effective dihedral derivative, $\partial C_l/\partial\beta$, deg^{-1}
$C_{l_{\delta_a}}$	differential aileron roll effectiveness derivative, $\partial C_l/\partial\delta_a$, deg^{-1}
$C_{l_{\delta_e}}$	differential elevon roll effectiveness derivative, $\partial C_l/\partial\delta_e$, deg^{-1}
$C_{l_{\delta_r}}$	rolling moment due to rudder deflection, $\partial C_l/\partial\delta_r$, deg^{-1}
C_n	yawing-moment coefficient, yawing moment/qsb
C_{n_p}	yawing moment due to roll rate, $\partial C_n/\partial(pb/2V)$, rad^{-1}
C_{n_r}	yawing damping derivative, $\partial C_n/\partial(rb/2V)$, rad^{-1}
C_{n_β}	directional stability derivative, $\partial C_n/\partial\beta$, deg^{-1}
$C_{n_{\delta_a}}$	yawing moment due to aileron deflection, $\partial C_n/\partial\delta_a$, deg^{-1}
$C_{n_{\delta_e}}$	yawing moment due to elevon deflection, $\partial C_n/\partial\delta_e$, deg^{-1}
$C_{n_{\delta_r}}$	rudder effectiveness derivative, $\partial C_n/\partial\delta_r$, deg^{-1}
CO	generalized control system output
C_Y	side force coefficient, side force/qs
C_{Y_p}	side force due to roll rate, $\partial C_Y/\partial p$, deg^{-1}
C_{Y_r}	side force due to yaw rate, $\partial C_Y/\partial r$, deg^{-1}
C_{Y_β}	side force due to sideslip, $\partial C_Y/\partial\beta$, deg^{-1}
$C_{Y_{\delta_a}}$	side force due to aileron deflection, $\partial C_Y/\partial\delta_a$, deg^{-1}
$C_{Y_{\delta_e}}$	side force due to elevon deflection, $\partial C_Y/\partial\delta_e$, deg^{-1}
$C_{Y_{\delta_r}}$	side force due to rudder deflection, $\partial C_Y/\partial\delta_r$, deg^{-1}
$\bar{c}$	mean aerodynamic chord, ft
cg	center of gravity, % $\bar{c}$ and FS
D	damping, lb sec/ft
$D_@$	damping of the arm, lb sec/ft
D_c	damping of the controller, lb sec/ft
D_i	damping of the wrist and hand interface, lb sec/ft
(e)	equivalent
F	force, lb
F_Y	lateral controller force, lb
F_{Y_c}	lateral controller force, lb
F_{Y_P}	lateral controller force pilot input, lb
F_{10}	roll-to-rudder gain schedule, $f(M)$
$f()$	function of parameter inside parentheses
I_X, I_Y, I_Z	vehicle moments of inertia, slug ft^2
I_{XZ}	product of inertia, slug ft^2

$j\omega$	imaginary part of Laplace transform variable, rad/sec
K	gain constant
$K_{@}$	arm spring constant, lb/ft
K_c	controller string constant, lb/ft
K_i	wrist spring constant, lb/ft
K_p	roll rate gain
l_x	longitudinal distance, ft
l_z	vertical distance, ft
m	aircraft mass, (lb-sec^2)/ft
$m_{@}$	mass of arm, (lb-sec^2)/ft
m_c	mass of controller, (lb-sec^2)/ft
p	rolling angular rate, deg/sec
$\dot{p}$	roll acceleration, deg/sec/sec
p_s	static atmospheric pressure, lb/ft^2
q	dynamic pressure, lb/ft^2
q_c	impact pressure, lb/ft^2
RI	generalized reference input
r	yawing angular rate, deg/sec
S	reference planform area, ft^2
s	Laplace transform variable, $(\sigma + j\omega)$, rad/sec
t	time, sec
V	true airspeed, ft/sec
W	weight, lb
$W_{@}$	weight of the arm, lb
$W_{@}(e)$	equivalent weight of the arm, lb
W_c	weight of the controller, lb
W_T	total weight of the controller plus added weight, lb
$W_T(e)$	total equivalent weight of the arm and controller, lb
x	output quantity
$x_{@}$	arm displacement, ft
x_c	transducer displacement, in. and ft
α	angle of attack, deg
β	angle of sideslip, deg
δ	control surface deflection, deg
ε	error signal
ζ	damping ratio
Δ	small change
$\Delta_{@}$	arm transfer function denominator
Δ_c	controller transfer function denominator
δ_a	differential aileron deflection, $(\delta_{a_R} - \delta_{a_L})/2$, deg
δ_e	differential elevon deflection, $(\delta_{e_R} - \delta_{e_L})/2$, deg
δ_r	rudder deflection, deg
θ	pitch altitude, deg
σ	real part of Laplace transform, rad/sec
ϕ	bank angle, deg
$\dot{\phi}_C/F_Y$	roll rate command gradient, (deg/sec)/lb
$\Delta\dot{\phi}_C/\Delta F_{Y_c}$	roll rate gradient gain, (deg/sec)/lb
ω	frequency, rad/sec
ω_{co}	crossover frequency, rad/sec
ω_d	damped frequency, rad/sec
ω_n	natural frequency, rad/sec
ω_r	ratcheting frequency, rad/sec
$\|$	absolute value
$\| d$B	amplitude ratio, dB

Sign Conventions

Trailing edge down is positive for δ_{a_L}, δ_{a_R}, δ_{e_L}, δ_{e_R}. Trailing edge left is positive for δ_r. Accelerations are positive forward, right, and down. Angles and rates are positive right wing down, nose up, and nose right. Angle of attack is positive with the nose (longitudinal axis) above the velocity vector. Angle of sideslip is positive with the nose left of the velocity vector.

Subscripts

@	arm
c	controller
D	damped
i	wrist interface
L	left
n	natural
o	trim condition
P	pilot
R	right

T	total
X, Y, Z	vehicle body axis
τ	tangential

Dot over quantity denotes first derivative with respect to time.

Dimensional Coefficients

The dimensional coefficients are defined as follows:

$$L_\beta = \frac{\bar{q}Sb}{I_X} C_{l_\beta}$$

$$N_\beta = \frac{\bar{q}Sb}{I_Z} C_{n_\beta}$$

$$Y_\beta = \frac{\bar{q}S}{mV} C_{Y_\beta}$$

$$L_p = \frac{\bar{q}Sb^2}{2VI_X} C_{l_p}$$

$$N_p = \frac{\bar{q}Sb^2}{2VI_Z} C_{n_p}$$

$$Y_p = \frac{\bar{q}Sb}{2mV^2} C_{Y_p} + \sin\alpha \approx \sin\alpha$$

$$L_{\delta_a, \delta_e, \delta_r} = \frac{\bar{q}Sb}{I_X} C_{l_{\delta_a, \delta_e, \delta_r}}$$

$$N_{\delta_a, \delta_e, \delta_r} = \frac{\bar{q}Sb}{I_Z} C_{n_{\delta_a, \delta_e, \delta_r}}$$

$$Y_{\delta_a, \delta_e, \delta_r} = \frac{\bar{q}S}{mV} C_{Y_{\delta_a, \delta_e, \delta_r}}$$

$$L_r = \frac{\bar{q}Sb^2}{2VI_X} C_{l_r}$$

$$N_r = \frac{\bar{q}Sb^2}{2VI_Z} C_{n_r}$$

$$Y_r = \frac{\bar{q}Sb}{2mV^2} C_{Y_r} - \cos\alpha \approx -\cos\alpha$$

APPENDIX B
DERIVATIVES AND AIRCRAFT PLANT FORMULATION

In general, the aircraft lateral–directional aerodynamic derivatives were obtained from either an average or the mean value of available flight data for a Mach number near 0.9.[3, 9, 10, 11] Wind-tunnel data were used in obtaining the control effectiveness of the elevon and aileron control derivatives.[12]

The coefficients listed in equation (B-1) were obtained with reference to the wind or stability axis. These coefficients provide the basic aerodynamics for generating the plant output and the integrated augmented aircraft response.

$$
\begin{aligned}
C_{l_\beta} &= -0.0016 \\
C_{n_\beta} &= 0.002 \\
C_{Y_\beta} &= -0.012 \\
C_{l_p} &= -0.24 \\
C_{n_p} &= -0.02 \\
C_{Y_p} &\quad (Y_p \approx \sin\alpha) \\
C_{l_r} &= 0.10 \\
C_{n_r} &= -0.2 \\
C_{Y_r} &= (Y_r \approx -\cos\alpha) \qquad \text{(B-1)} \\
C_{l_{\delta_a}} &= -0.0013 \\
C_{n_{\delta_a}} &= -0.0005 \\
C_{Y_{\delta_a}} &= 0.002 \\
C_{l_{\delta_e}} &= -0.0011 \\
C_{n_{\delta_e}} &= -0.0007 \\
C_{Y_{\delta_e}} &= 0.002 \\
C_{l_{\delta_r}} &= 0.0003 \\
C_{n_{\delta_r}} &= -0.0006 \\
C_{Y_{\delta_r}} &= 0.001
\end{aligned}
$$

First, it was necessary to translate the coefficients from the stability to the body axis and then convert to the dimensional coefficients (eq. (B-2)) using the flight data and the physical characteristics (table 2).

$$
\begin{aligned}
L_\beta &= \frac{\bar{q}Sb}{I_X} C_{l_\beta} \\
N_\beta &= \frac{\bar{q}Sb}{I_Z} C_{n_\beta} \\
Y_\beta &= \frac{\bar{q}S}{mV} C_{Y_\beta} \\
L_p &= \frac{\bar{q}Sb^2}{2VI_X} C_{l_p} \\
N_p &= \frac{\bar{q}Sb^2}{2VI_Z} C_{n_p} \\
Y_p &= \sin\alpha \\
L_{\delta_a, \delta_e, \delta_r} &= \frac{\bar{q}Sb}{I_X} C_{l_{\delta_a, \delta_e, \delta_r}} \qquad \text{(B-2)} \\
N_{\delta_a, \delta_e, \delta_r} &= \frac{\bar{q}Sb}{I_Z} C_{n_{\delta_a, \delta_e, \delta_r}} \\
Y_{\delta_a, \delta_e, \delta_r} &= \frac{\bar{q}S}{mV} C_{Y_{\delta_a, \delta_e, \delta_r}} \\
L_r &= \frac{\bar{q}Sb^2}{2VI_X} C_{l_r} \\
N_r &= \frac{\bar{q}Sb^2}{2VI_Z} C_{n_r} \\
Y_r &= -\cos\alpha
\end{aligned}
$$

Using the state-space notation, the lateral–directional equations can be arranged initially in a matrix format as

$$C\dot{x} = Ax + Bu$$

$$\begin{bmatrix} 1 & 0 & 0 & 0 \\ 0 & 1 & -\frac{I_{XZ}}{I_X} & 0 \\ 0 & -\frac{I_{XZ}}{I_Z} & 1 & 0 \\ 0 & 0 & 0 & 1 \end{bmatrix} \begin{bmatrix} \dot{\beta} \\ \dot{p} \\ \dot{r} \\ \dot{\phi} \end{bmatrix} = \begin{bmatrix} Y_\beta & \sin\alpha & -\cos\alpha & \frac{g}{V_o}\cos\theta_0 \\ L_\beta & L_p & L_r & 0. \\ N_\beta & N_p & N_r & 0. \\ 0. & 1.0 & \tan\theta_0 & 0. \end{bmatrix} \begin{bmatrix} \beta \\ p \\ r \\ \phi \end{bmatrix}$$

$$+ \begin{bmatrix} Y_{\delta_a} & Y_{\delta_r} & Y_{\delta_e} \\ L_{\delta_a} & L_{\delta_r} & L_{\delta_e} \\ N_{\delta_a} & N_{\delta_r} & N_{\delta_e} \\ 0. & 0. & 0. \end{bmatrix} \begin{bmatrix} \delta_a \\ \delta_r \\ \delta_e \end{bmatrix}$$

$$y = Hx + G\dot{x} \qquad \text{(B-3)}$$

$$\begin{bmatrix} \beta \\ p \\ r \\ \phi \\ a_{Y_s} \end{bmatrix} = \begin{bmatrix} 1 & 0 & 0 & 0 \\ 0 & 1 & 0 & 0 \\ 0 & 0 & 1 & 0 \\ 0 & 0 & 0 & 1 \\ 0 & -\frac{V_o}{g}\sin\alpha_0 & \frac{V_o}{g}\cos\alpha_0 & -\cos\theta_0 \end{bmatrix} \begin{bmatrix} \beta \\ p \\ r \\ \phi \end{bmatrix} + \begin{bmatrix} 0 & 0 & 0 & 0 \\ 0 & 0 & 0 & 0 \\ 0 & 0 & 0 & 0 \\ 0 & 0 & 0 & 0 \\ \frac{V_o}{g} & -\frac{l_Z}{g} & \frac{l_X}{g} & 0 \end{bmatrix} \begin{bmatrix} \dot{\beta} \\ \dot{p} \\ \dot{r} \\ \dot{\phi} \end{bmatrix}$$

The plant output quantities (y) as a function of the input functions (u) can be reduced simply to

$$\dot{x} = A'x + B'u$$
$$y = Hx + G\dot{x}$$

Where the prime indicates premultiplication by C^{-1},

$$\dot{x} = A'x + B'u$$

$$\begin{bmatrix} \dot{\beta} \\ \dot{p} \\ \dot{r} \\ \dot{\phi} \end{bmatrix} = \begin{bmatrix} Y_\beta & \sin\alpha & -\cos\alpha & \frac{g}{V_{T_0}}\cos\theta_0 \\ L_\beta & L_p & L_r & 0. \\ B_\beta & N_p & N_r & 0. \\ 0. & 1.0 & \tan\theta_0 & 0. \end{bmatrix} \begin{bmatrix} \beta \\ p \\ r \\ \phi \end{bmatrix} + \begin{bmatrix} Y_{\delta_a} & Y_{\delta_r} & Y_{\delta_e} \\ L_{\delta_a} & L_{\delta_r} & L_{\delta_e} \\ N_{\delta_a} & N_{\delta_r} & N_{\delta_e} \\ 0. & 0. & 0. \end{bmatrix} \begin{bmatrix} \delta_a \\ \delta_r \\ \delta_e \end{bmatrix}$$

$$y = Hx + G\dot{x} \qquad \text{(B-4)}$$

$$\begin{bmatrix} \beta \\ p \\ r \\ \phi \\ a_{Y_s} \end{bmatrix} = \begin{bmatrix} 1 & 0 & 0 & 0 \\ 0 & 1 & 0 & 0 \\ 0 & 0 & 1 & 0 \\ 0 & 0 & 0 & 1 \\ 0 & -\frac{V_o}{g}\sin\alpha_0 & \frac{V_o}{g}\cos\alpha_0 & -\cos\theta_0 \end{bmatrix} \begin{bmatrix} \beta \\ p \\ r \\ \phi \end{bmatrix} + \begin{bmatrix} 0 & 0 & 0 & 0 \\ 0 & 0 & 0 & 0 \\ 0 & 0 & 0 & 0 \\ 0 & 0 & 0 & 0 \\ \frac{V_o}{g} & -\frac{l_Z}{g} & \frac{l_X}{g} & 0 \end{bmatrix} \begin{bmatrix} \dot{\beta} \\ \dot{p} \\ \dot{r} \\ \dot{\phi} \end{bmatrix}$$

The complete computational procedure, including the axis rotation, is accomplished by using a FORTRAN program developed at the NASA Dryden Flight Research Center. Numerical values for the matrix coefficients A', B', H, and G at the example flight conditions are presented as equation (B-5).

$$A' = \begin{bmatrix} -.4172 & .0523 & -.9986 & .0333 \\ -73.172 & -3.0602 & 1.2365 & 0. \\ 15.1645 & -.0369 & -.4511 & 0. \\ 0. & 1.0 & .0524 & 0. \end{bmatrix}$$

$$B' = \begin{bmatrix} 0.071 & .0348 & .0695 \\ -54.285 & 14.267 & -45.26 \\ -4.152 & -4.588 & -5.659 \\ 0. & 0. & 0. \end{bmatrix} \qquad \text{(B-5)}$$

$$H = \begin{bmatrix} 1. & 0. & 0. & 0. \\ 0. & 1. & 0. & 0. \\ 0. & 0. & 1. & 0. \\ 0. & 0. & 0. & 1. \\ 0. & -1.567 & 29.92 & -.998 \end{bmatrix}$$

$$G = \begin{bmatrix} 0. & 0. & 0. & 0. \\ 0. & 0. & 0. & 0. \\ 0. & 0. & 0. & 0. \\ 0. & 0. & 0. & 0. \\ 29.93 & 0. & .53 & 0. \end{bmatrix}$$

The final linearized numerical matrix coefficients (eq. (B-5)) are a suitable aerodynamic state-space representation for integration into the FORTRAN control program.[13] Output-dependent variables of the aerodynamic plant provide the rates and accelerations necessary for augmenting the aircraft.

APPENDIX C
MINIMUM DISPLACEMENT CONTROLLER DYNAMICS

The F-16 XL-2 aircraft was constructed with a dual cockpit during the modification and assembly. Both crew members are provided with identical two-axes, pedestal-mounted, minimum displacement controllers that are located on the right side of the cockpit. The controller is positioned slightly forward of the center of gravity of the pilot's body to permit a semi-relaxed arm position.

In both axes, the controller senses displacement measured through the transducer displaced by force up to a maximum displacement of ±0.25 in. The transducer is calibrated in lb. A breakout force of 1 lb is required before any displacement results. The spring constant up to the maximum deflection is approximately 960 lb/ft (fig. C-1).

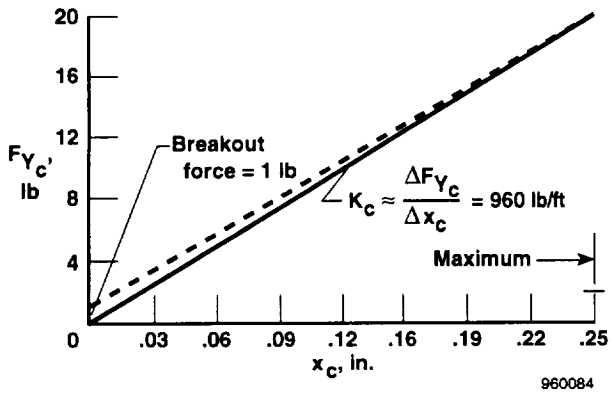

Figure C-1. Spring gradient of the minimum displacement controller.

To get some idea of the dynamic response of the controller as a function of mass, extra weights were added by wrapping lead strips around the controller grip. The controller, W_c, weighs 1.25 lb.

The controller was pulled to maximum deflection and released. Figure C-2 shows a typical response for a total weight, W_T, of 5.18 lb (W added = 3.93 lb). For this particular weight and test, the controller exhibited a damped frequency, ω_d, of 76.6 rad/sec at a damping ratio, ζ, of 0.09 following the release.

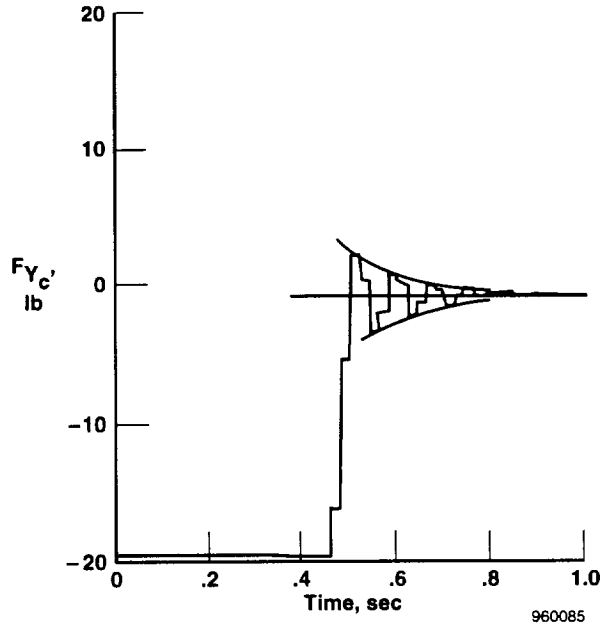

Figure C-2. Typical controller response following a F_{Y_c} = 20 lb release: W_T = 5.18 lb, period = 0.082 sec, ω_d = 76.6 rad/sec, ζ = 0.09 and K_c = 960 lb/ft.

Figure C-3 shows a summary of this test and two additional test weight conditions. For the controller alone (W_c = 1.25 lb), the release results in no overshoot. A dashed line is drawn through the damping ratio data points. A constant value of damping force (D_c = 2.24 (lb-sec)/ft was used to estimate the damping ratio from 5.18 to 9 lb. The solid line on the frequency figure indicates the natural frequency by using $\omega_n = \sqrt{K_c g / W_T}$. The two data points were the damped frequency obtained from the response for the indicated added total weight.

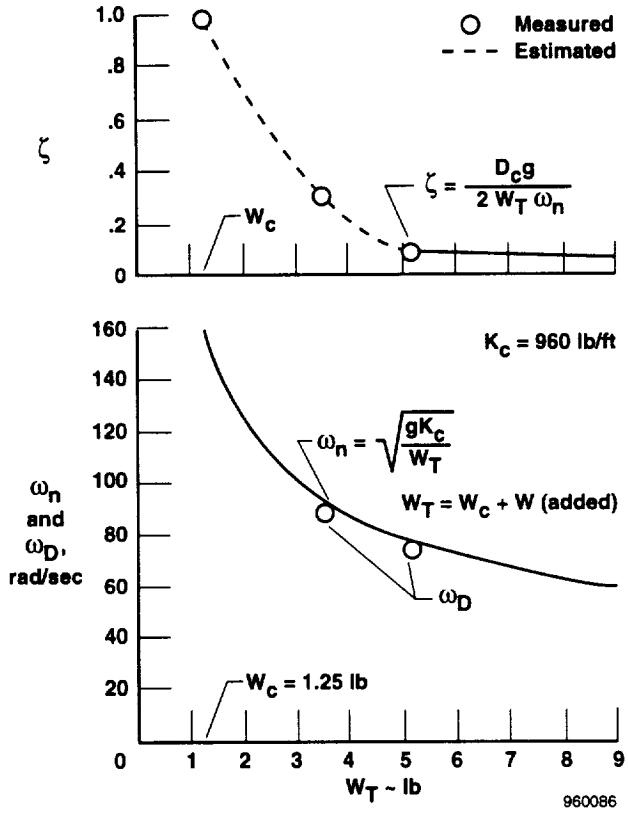

Figure C-3. Controller frequency and damping as a function of total weight, W_c + W(added).

APPENDIX D
BIOMECHANICAL MODELING AND MANIPULATION DYNAMICS

The following description, derivations, and modeling aspects of the "bobweight" effects rely heavily on the experimental and analytical studies.[10] A large vibration platform was used on which a control operator was restrained at the seat to the platform. The platform was subjected to lateral accelerations ranging in frequencies from 0 to 10 Hz. The operator performed isolated-axis-displayed control tasks. Two types of center-stick controllers were mounted on the platform: a spring stick and a stiff stick. These controllers were investigated throughout the lateral control tests. From these experiments, the most significant modal responses were derived from the biomechanical nature of the arm/muscle coupled through the hand/grip interface to the controller.

Figure D-1 shows a biomechanical model, showing the lateral forces and accelerations, and a mathematical description of the dynamic elements.[10] The directions of the forces, accelerations, and displacements are defined as positive to the right. Consider a minimum displacement controller, K_c = 960 lb/ft, with aircraft accelerations measured in g and the mass properties defined in terms of equivalent or effective weights (fig. D-1). The forces and elements can be summed and resolved as two equations with two unknowns, x_c and $x_{@}$.

$$[m_c s^2 + (D_i + D_c)s + K_i + K_c]x_c - (D_i s + K_i)x_{@} = W_c(-a_{Y_\tau}) \tag{D-1}$$

$$-(D_i s + K_i)x_c + [m_{@} s^2 + (D_i + D_{@})s + K_i + K_{@}]x_{@} = W_{@}(e)(-a_{Y_\tau}) + F_{Y_P} \tag{D-2}$$

or

$$[\Delta_c + (D_i s + K_i)]x_c - (D_i s + K_i)x_{@} = W_c(-a_{Y_\tau}) \tag{D-3}$$

$$-(D_i s + K_i)x_c + [\Delta_{@} + (D_i s + K_i)]x_{@} = W_{@}(e)(-a_{Y_\tau}) + F_{Y_P} \tag{D-4}$$

where

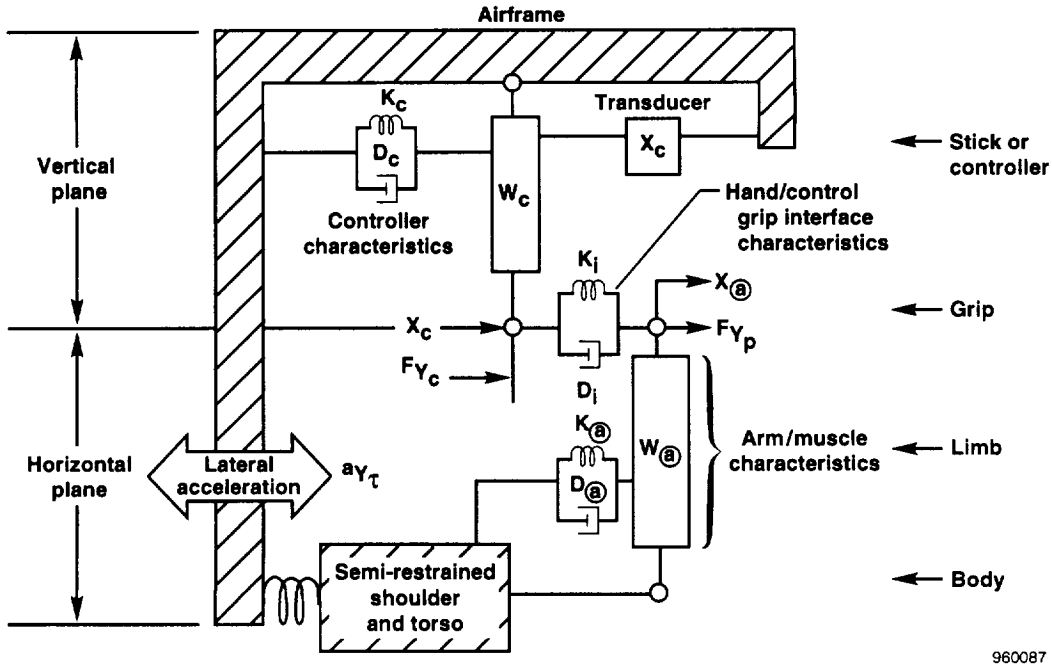

Figure D-1. Feedthrough mechanical controller model with lateral force and acceleration input.[10]

$$\Delta_c = m_c s^2 + D_c s + K_c$$
$$\Delta_@ = m_@ s^2 + D_@ s + K_@$$
$$m_c = W_c/g$$
$$m_@ = W_@(e)/g$$

Solving equations (D-3) and (D-4) for $x_@$ and combining gives the following equation for the biodynamics:

$$\frac{x_c}{-a_{Y_\tau}} = \frac{F_{Y_P}(D_i s + K_i)/-a_{Y_\tau} + (D_i s + K_i)(W_@(e) + W_c) + \Delta_@ W_c}{(D_i s + K_i)(\Delta_@ + \Delta_c) + \Delta_@ \Delta_c} \quad \text{(D-5)}$$

However, Δ_c is much larger than $\Delta_@$; therefore, $\Delta_@ + \Delta_c \approx \Delta_c$. For the lower frequency range of interest, $\omega < 30$ rad/sec, Δ_c can be approximated by the controller spring constant, K_c. Equation (D-6) then becomes (for a positive a_{Y_τ}) as follows:

$$\frac{x_c}{a_{Y_\tau}} = \frac{F_{Y_P}(D_i s + K_i)/a_{Y_\tau}}{K_c[(D_i s + K_i) + \Delta_@]} - \frac{(D_i s + K_i)(W_@(e) + W_c)}{K_c[(D_i s + K_i) + \Delta_@]} - \frac{\Delta_@ W_c}{K_c[(D_i s + K_i) + \Delta_@]} \quad \text{(D-6)}$$

Equation (D-6) can be represented as a feedthrough system with tangential acceleration a_{Y_τ} at the controller as the input and F_{Y_c} as the output (fig. D-2).

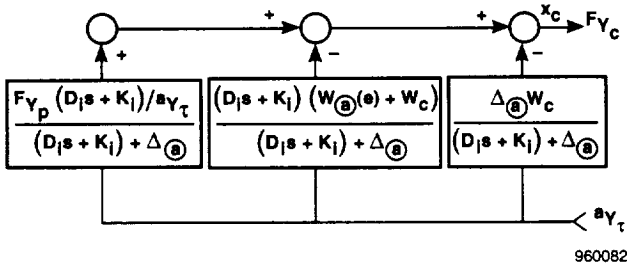

Figure D-2. Representation of equation (D-6).

For simplification, the initial and end blocks can be thought of as unity where $K_c = \frac{\Delta F_{Y_c}}{\Delta x_c}$ (fig. (C-1)).

The feedback block, $D_i s + K_i/(D_i s + K_i) + \Delta_@$, can be further moved to the forward loop and simplified to a block diagram with F_{Y_P} and a_{Y_τ} as the inputs and F_{Y_c} as the output or input to the roll command gradient (fig. (D-3)).

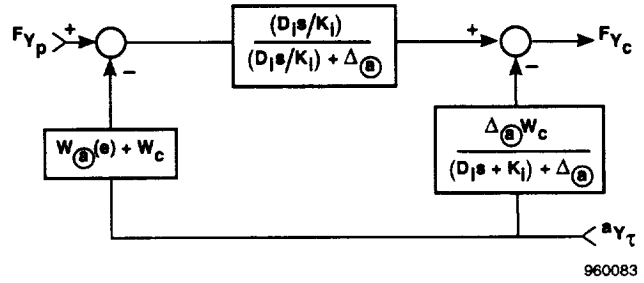

Figure D-3. Equivalent representation of figure (D-2) with pilot input.

Measured values for the coefficients and gains were determined from vibration tests as (ref. 10)

$$K_@ = 9.46 \text{ lb/ft}$$
$$K_i = 24.26 \text{ lb/ft}$$
$$D_@ = 0.61 \text{ (lb-sec)/ft}$$
$$D_i = 2.09 \text{ (lb-sec)/ft} \quad \text{(D-7)}$$
$$\frac{K_i}{K_@ + K_i} = 0.72$$
$$\frac{K_@}{K_@ + K_i} = 0.28$$

The equivalent weight for the controller is

$$W_c = 1.25 \text{ lb} \quad \text{(D-8)}$$

The dynamic response of the controller was approximated by the spring constant, $K_c = 960$ lb/ft. The measured dynamic characteristics are presented in appendix C.

APPENDIX E
DUAL LAG EQUIVALENT TRANSFER FUNCTION

All F-16 aircraft have a unique feedback system device in the forward command path referred to as a dual lag. This device provides for a softer roll-in and a sharper rollout command, thereby minimizing the tendency to overshoot. Figure E-1 shows the analog system as excerpted from the functional block diagram[14] describing the roll system of the F-16 XL airplane.

A bias of ±20 deg/sec exists on the feedback C. Hence, any output within that range would be derived simply by computing $CO = 10RI/(s + 10)$. For outputs greater than ±20 deg/sec, the output would be modified by the feedback functions to the extent of the output exceeding the bias.

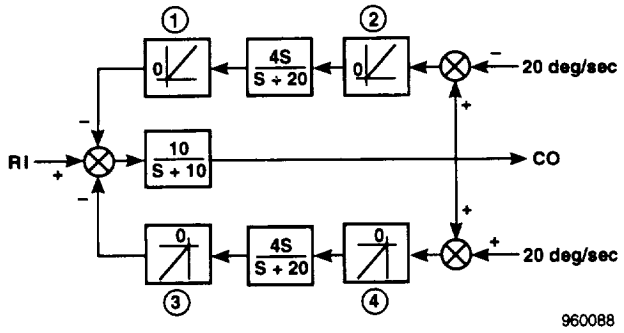

Figure E-1. The nonlinear dual-lag system.

The commanded roll rate and bias become important considerations as noted with reference to the roll ratcheting experienced, described, and analyzed in this report (fig. 5 and 6). The oscillation is initially biased at an offset near –60 deg/sec. In addition, the oscillation varies ±10 deg/sec about the offset at the ratcheting frequency near 16.4 rad/sec. For one-half cycle, where $(CO + \Delta CO) < -60$ deg/sec, the output/input would be as follows:

$$\left[\frac{CO}{RI}\right]_{\frac{1}{2}\text{ cycle}} = \frac{10(s + 20)}{(s + 3)(s + 67)} \tag{E-1}$$

Because the diode ③ is downstream of the washout, for the rest of the cycle and for $(CO + \Delta CO) > -60$ deg/sec, the response would be as follows:

$$\left[\frac{CO}{RI}\right]_{\frac{1}{2}\text{ cycle}} = \frac{10}{(s + 10)} \tag{E-2}$$

Consequently, for sinusoidal inputs, a piecewise description of the output would be required. However, to avoid employing the complexity of using describing functions, which would result in a derivation as a function of frequency and amplitude, a linear compromise was considered sufficient for determining the amplitude and phase. Figure E-2 shows this compromise with just the asymptotes depicting the transfer functions.

The two dashed lines, as indicated, represent the two transfer functions $10/(s + 10)$ and $10(s + 20)/(s + 3)(s + 67)$. The solid line represents the linear compromise:

$$\frac{CO}{RI} = \frac{10(s + 40)}{(s + 6)(s + 67)} \tag{E-3}$$

At the ratcheting frequency, 16.4 rad/sec, this function will give a linear amplitude ratio of 0.358 and a phase angle of –61.33°. The actual amplitude ratio is pointed out by the asterisk. The amplitude ratios of the two other functions are indicated by the small circles at the ratcheting frequency.

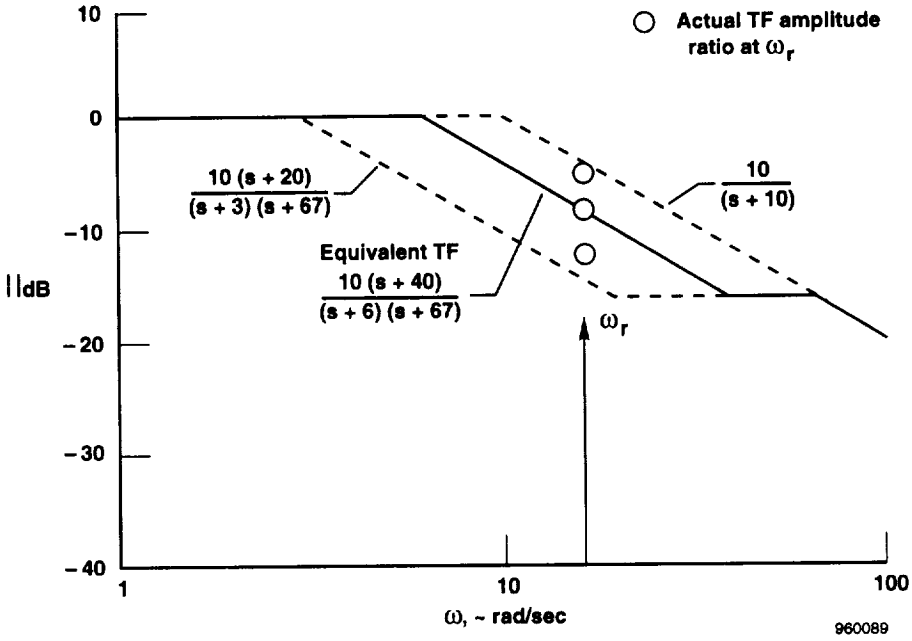

Figure E-2. Asymptotic approximations of the dual-lag transfer functions.

REFERENCES

[1]Bailey, R. E. And Knotts, L. H., *Interaction of Feel System and Flight Control Dynamics on Lateral Flying Qualities*, NASA CR-179445, 1990.

[2]Hall, G. Warren and Smith, Rogers E., *Flight Investigation of Fighter Side-Stick Force-Deflection Characteristics*, AFFDL-TR-75-39, May 1975.

[3]Scofield, Jan W., Scott, Sheryl R., and Thomas, Edwin A., *F16XL Phase 1 Flying Qualities Evaluation*, AFFTC-TR-83-26, Sep. 1983.

[4]Monagan, Stephen J., Smith, Rogers E., and Bailey, Randall E., *Lateral Flying Qualities of Highly Augmented Fighter Aircraft*, AFWAL-TR-81-3171, vol. I, Mar. 1982.

[5]Chalk, C. R., "Excessive Roll Damping Can Cause Roll Ratchet," *Journal of Guidance, Control and Dynamics*, vol. 6, May–June 1983, pp. 218–219.

[6]McRuer, D. T. and Magdaleno, R. E., *Human Pilot Dynamics With Various Manipulators*, AFFDL-TR-66-138, Dec. 1966.

[7]Johnston, Donald E. and Aponso, Bimal L., *Design Considerations of Manipulator and Feel System Characteristics in Roll Tracking*, NASA CR-4111, 1988.

[8]Magdaleno, R. E. and McRuer, D. T., *Experimental Validation and Analytical Elaboration for Models of the Pilot's Neuromuscular Subsystem in Tracking Tasks*, NASA CR-1757, 1971.

[9]Johnston, D. E. and McRuer D. T., *Investigation of Interactions Between Limb-Manipulator Dynamics and Effective Vehicle Roll Control Characteristics*, NASA CR-3983, 1986.

[10]Allen, R. Wade, Jex, Henry R., and Magdaleno, Raymond E., *Manual Control Performance and Dynamic Response During Sinusoidal Vibration*, STI TR-1013-2, Oct. 1973.

[11]Tierney, Sheryl S. and Thomas, Edwin A., *F-16XL Follow-On Development Flying Qualities Evaluation*, AFFTC-TR-85-31, Nov. 1985.

[12]Humphries, John A. and Caughlin, Donald J., *F-16XL Flying Qualities With the Large Normal Shock Inlet*, AFFTC-TR-85-34, Feb. 1986.

[13]Loman, R. B., Wilson, J. W., and Johnson, S. D., *F-16XL Stability and Control Flight Test Report*, 400PR106, Addendum I, Dec. 1985.

[14]von Bose, D. R., Tierney, P. K., and Wilson, J. W., *F-16XL Stability and Control Data Substantiation Report*, 400PR050, May 1982.

[15]Edwards, John W., *A FORTRAN Program for the Analysis of Linear Continuous and Sampled-Data Systems*, NASA TM-X-56038, 1976.

[16]Forgey, D. H., Wilde, W. C., and Weis, N. N., *F-16XL Flight Control System Description Report*, 400PR042, Dec. 1985.

[17]Krogman, Wilton Marion and Johnston, Francis E., *Human Mechanics: Four Monographs Abridged*, AMRL-TDR-63-123, Dec. 1963.

REPORT DOCUMENTATION PAGE

Form Approved
OMB No. 0704-0188

1. AGENCY USE ONLY (Leave blank)	2. REPORT DATE	3. REPORT TYPE AND DATES COVERED
	July 1996	Technical Memorandum

4. TITLE AND SUBTITLE

Biomechanically Induced and Controller Coupled Oscillations Experienced on the F-16XL Aircraft During Rolling Maneuvers

5. FUNDING NUMBERS

WU 505-68

6. AUTHOR(S)

John W. Smith and Terry Montgomery

7. PERFORMING ORGANIZATION NAME(S) AND ADDRESS(ES)

NASA Dryden Flight Research Center
P.O. Box 273
Edwards, California 93523-0273

8. PERFORMING ORGANIZATION REPORT NUMBER

H-2031

9. SPONSORING/MONOTORING AGENCY NAME(S) AND ADDRESS(ES)

National Aeronautics and Space Administration
Washington, DC 20546-0001

10. SPONSORING/MONITORING AGENCY REPORT NUMBER

NASA TM-4752

11. SUPPLEMENTARY NOTES

12a. DISTRIBUTION/AVAILABILITY STATEMENT

Unclassified—Unlimited
Subject Category 08

12b. DISTRIBUTION CODE

13. ABSTRACT (Maximum 200 words)

During rapid rolling maneuvers, the F-16 XL aircraft exhibits a 2.5 Hz lightly damped roll oscillation, perceived and described as "roll ratcheting." This phenomenon is common with fly-by-wire control systems, particularly when primary control is derived through a pedestal-mounted sidearm controller. Analytical studies have been conducted to model the nature of the integrated control characteristics. The analytical results complement the flight observations. A three-degree-of-freedom linearized set of aerodynamic matrices was assembled to simulate the aircraft plant. The lateral–directional control system was modeled as a linear system. A combination of two second-order transfer functions was derived to couple the lateral acceleration feedthrough effect of the operator's arm and controller to the roll stick force input. From the combined systems, open-loop frequency responses and a time history were derived, describing and predicting an analogous in-flight situation. This report describes the primary control, aircraft angular rate, and position time responses of the F-16 XL-2 aircraft during subsonic and high-dynamic-pressure rolling maneuvers. The analytical description of the pilot's arm and controller can be applied to other aircraft or simulations to assess roll ratcheting susceptibility.

14. SUBJECT TERMS

Biomechanics; F-16XL airplane; Flying qualities; Handling qualities; Human factors; Pilot induced oscillations; Roll control; Roll ratcheting

15. NUMBER OF PAGES

38

16. PRICE CODE

AO3

17. SECURITY CLASSIFICATION OF REPORT	18. SECURITY CLASSIFICATION OF THIS PAGE	19. SECURITY CLASSIFICATION OF ABSTRACT	20. LIMITATION OF ABSTRACT
Unclassified	Unclassified	Unclassified	Unlimited

NSN 7540-01-280-5500

Available from the NASA Center for AeroSpace Information, 800 Elkridge Landing Road, Linthicum Heights, MD 21090; (301)621-0390

Standard Form 298 (Rev. 2-89)
Prescribed by ANSI Std. Z39-18
298-102